PROCEEDINGS A

royalsocietypublishing.org/journal/rspa

Research

Cite this article: Mariano PM, Planas J, Radi E, Salvatori L, Martin Stickle M. 2026 Subsonic propagation of cracks between dissimilar quasicrystals. *Proc. R. Soc. A* **482**: 20250608. https://doi.org/10.1098/rspa.2025.0608

Received: 11 July 2025
Accepted: 17 November 2025

Subject Areas:
mathematical physics, mechanics, applied mathematics

Keywords:
continuum mechanics, bi-material interfaces, fracture, quasicrystals

Author for correspondence:
Paolo Maria Mariano
e-mail: paolomaria.mariano@unifi.it

Subsonic propagation of cracks between dissimilar quasicrystals

Paolo Maria Mariano[1], Jaime Planas[2], Enrico Radi[4], Luca Salvatori[1] and Miguel Martin Stickle[3]

[1]DICEA, Università di Firenze, via Santa Marta 3, Firenze 50139, Italy
[2]Department of Materials Science, and [3]Departamento de Matemática e Informática Aplicadas a las Ingenierías Civil y Naval, ETSI Caminos, Canales y Puertos, Universidad Politécnica de Madrid, Profesor Aranguren s/n, Madrid 28040, Spain
[4]DiSMI, Università di Modena e Reggio Emilia, via Amendola 2, Reggio Emilia 42122, Italy

PMM, 0000-0002-3841-8408

We analyse the subsonic propagation of a crack along the interface between two different quasicrystals in a two-dimensional (2D) ambient setting and small strain regime. In the absence of a phason self-action, we provide a closed-form solution of the related Riemann–Hilbert problem. Then, we use such a result as a benchmark for a numerical analysis of the influence of a phason self-action on the crack propagation, which is the focus of our work. In addition to the special attention to quasicrystals, our work extends the classical analyses of interface cracks in linear elasticity to more general elastic bodies with 'active' microstructure described by vector phase fields.

1. Introduction

We consider a fracture between two adherent dissimilar elastic quasicrystals. We analyse its equilibrium and subsonic propagation in different conditions.

Attention to the emergence of fractures at interfaces is in general justified by the frequent recurrence of the phenomenon in solids and its influence on the gross behaviour [1–3].

In the case of quasicrystals, there are more specific reasons. Quasicrystals are Al–Mn-based alloys whose atomic aggregates have point group symmetry that is inconsistent with lattice translation. They were revealed first in 1984 [4]. Their atomic lattice is intrinsically

THE ROYAL SOCIETY PUBLISHING

quasi-periodic. It differs from a periodic atomic array by the presence of topological alterations determined by clusters of atoms with point group symmetry different from the prevailing one. Local rearrangements, owing to jumps of atoms between neighbouring places and/or collective atomic modes, generated by the flipping of crisscrossing alterations needed to maintain matching rules [5–7], determine quasi-periodicity. They do not have specific location. 'Even if a quasicrystal is energetically stabilized representing a ground state, it was shown numerically that above some critical temperature the system is in a random-tiling-like phase or unlocked phase' [5]. Quasicrystals display a much lower toughness than metals, approximately two orders of magnitude smaller. They have scarce resistance to crack propagation at temperatures below 450°C [8], where their behaviour is essentially brittle, while at elevated temperatures they show extensive ductility, apparently with no significant hardening. They are predominantly used as surface coatings or composites owing to their hardness, low thermal conductivity, low surface energy and low friction; mechanical integrity is provided by the substrate or matrix, whereas the quasicrystal offers supplemental functions such as hardness, protection against corrosion, optical absorbance, etc. In the case of surface coatings, their use combines wear resistance with low friction and/or low adhesion, so that they are competitive with Teflon (their hardness is in fact greater than that of Teflon). They allow the use of normal cutlery with quasicrystal coatings. In particular, for cookware, quasicrystal coatings can advantageously replace Teflon, since their low thermal conductivity leads to even surface heating [8]. In this technological ambient setting, interfacial cracks are recurrent.

Our analysis extends results concerning interfacial cracks between dissimilar simple elastic-brittle bodies. We clarify further the difference between a complete formulation of the linear elasticity of quasicrystals and its simplification based on neglecting the phason self-action. Indeed, quasicrystals cannot be considered simple bodies in the traditional sense of Noll. Instead, their representation falls within the class of materials that we can call *complex* because they experience observable internal degrees of freedom with related bulk and contact actions.

A well-known example of planar quasi-periodic covering is Penrose tiling; it replicates in dual way the structure of a quasi-periodic lattice, which can be considered as the projection of a higher-dimensional periodic lattice over an incommensurate low-dimensional subspace. A simple example that we find often repeated is to consider in the plane a square lattice and a line inclined by an irrational angle with respect to the symmetry axes of the square. If we consider a wide strip around the line and project the mass points inside it orthogonally over the line itself, we obtain a one-dimensional lattice. This picture has an analytical basis. In fact, if we expand in Fourier series the mass distribution of a three-dimensional (3D) quasi-periodic lattice, the resulting wave vectors are six-dimensional [9].

The additional degrees of freedom revealed by the Fourier analysis must be considered at the continuum scale as internal to every material element, which—identified with a point at the scale considered—has only three degrees of freedom in the 3D physical space. This scenario can be profitably represented by two space-time dependent differentiable fields:

— the *displacement* $(y,t) \longmapsto u := \tilde{u}(y,t) \in \mathbb{R}^3$; and
— the so-called *phason field* $(y,t) \longmapsto \nu := \tilde{\nu}(y,t) \in \hat{\mathbb{R}}^3$, which collects the inner degrees of freedom evidenced by the Fourier analysis on quasi-periodic lattices.

The word 'phason' recalls that ν describes in time and space the potential local phase rearrangement of the atomic clusters needed for assuring quasi-periodicity. Since ν represents degrees of freedom that are inner to every material element at continuum scale (see the sketch in figure 1), they are insensitive to Galilean (that is, translational) changes of observers in physical space, while they are sensitive to the rotational changes of observers. True interactions are associated with the phason field; they are defined by the power that they perform in the time rate of ν. They are subdivided as usual into bulk and contact families. Their balance equations—which complement those of standard (deformational) forces—can be derived by imposing invariance of the power exerted on a generic body part (so, the external power) under rigid-body type changes

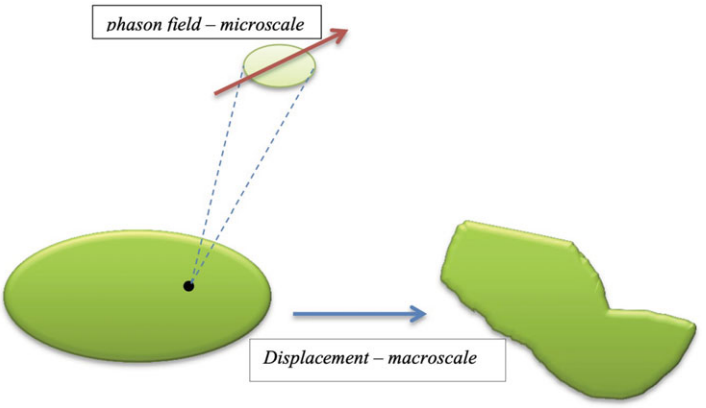

Figure 1. Distinction between displacement (also called phonon field) and phason field; they act at different scales; ν is approximately 1/100 of u.

of observers, as shown in [10,11]. They can be also derived from a d'Alembert–Lagrange principle, which allows one to also include dissipative effects [12]. In this case, however, we put on the same level balances of interactions and constitutive prescriptions (at least with respect to the specification of state variables), while we know that the former are independent of the latter. Another path to be followed in a purely dissipative setting is to require structure invariance of the Clausius–Duhem inequality (written including the external power and not the internal one) under generic diffeomorphim-based changes of observer; the choice allows one to obtain the representation of contact actions in terms of stress, the local balance equations and constitutive restrictions; this approach, based on covariance, has been proposed for general complex bodies in [13]. From all these viewpoints, the insensitivity of ν to Galilean changes of observers—those determined only by rigid translations in the physical space—implies the existence of a phason self-action. It is often neglected in the elasticity of quasicrystals only for analytical convenience (several examples are available; we just mention the treatise [14] and, for the specific analysis of fractures, references [15–19]) but this is only a particular constitutive choice—and surely an admissible one, but a special choice, in fact. However, a conservative component of the phason self-action may have non-trivial influence on the material stability, as shown in [20]. To investigate further its role, we focus here on the small strain regime and comparatively evaluate how the presence of a conservative component of the phason self-action influences the description of interfacial cracks between dissimilar quasicrystals. Various analyses on interfacial cracks in quasicrystals have been proposed [15,16,19,21–26]; however, they do not include a discussion on the occurrence and effects of the phason self-action. This last aspect is the main focus of the present paper. Providing this type of comparative analyses establishes a ground for laboratory experiments aiming at recording the distribution of stresses, possibly by means of photoelastic procedures. These kind of experiments might determine whether the special choice of neglecting a conservative phason self-action could have a universal character or not.

We act in a two-dimensional (2D) ambient space filled by a bi-material planar body: two different quasi-crystalline alloys, one for each half-plane. The two materials are attached along a planar coherent interface where there is a semi-infinite crack $\mathcal{C}$. Figure 3 describes the situation. A frame of reference is chosen as in figure 3. It is attached at the crack tip and refers to material axes; in particular, the x_1-axis corresponds to a 'plane' of pentagonal symmetry for both the quasicrystals on either side of the interface. Our attention is focused on the elastic behaviour in linearized setting. Dissipation can occur only at the crack tip when it proceeds along the interface.

First, we consider the absence of phason self-action. In this case, we provide a closed-form solution of the stress profiles around the crack tip when the crack margins are not loaded and the bulk actions are neglected; the analysis is developed using Stroh formalism [27], a

complex variable representation of balance equations in 2D linear elasticity. From an analytical viewpoint, the bi-material character of the body implies a degenerate eigenvalue problem, which requires modifications of the Stroh approach [28] (see also [29–31] for the way to tackle analytical difficulties in the presence of bi-material bodies).

Then, we consider the presence of a conservative self-action and analyse the mechanical response around the tip in mode I conditions, using finite elements. Comparison with the analytical results shows qualitatively and quantitatively the incidence of the phason self-action on the overall mechanical behaviour. Finally, we discuss the structure of configurational actions at the crack tip along the interface.

Regarding notation, an interposed dot is used for the scalar product between elements of a linear space, whatever its nature. A superposed dot denotes the time derivative, while the superscript $\top$ indicates standard transposition. For simplicity, we refer all analyses to orthonormal frames of reference, so that we do not distinguish between covariant and contravariant components of the linear operators, that is, between vectors and covectors.

2. A summary of the mechanics of quasicrystals in long-wavelength approximation

(a) Displacement and phason fields

Consider two identical copies of the 3D real space, say $\mathbb{R}^3$ and $\tilde{\mathbb{R}}^3$; the former is a reference space, the latter is the physical space. In $\mathbb{R}^3$, we select a reference configuration $\mathcal{B}$, which is an open, bounded, connected set with surface-like boundary oriented by the outward unit normal to within a finite number of corners and edges. With x we indicate a generic point in $\mathcal{B}$. Deformed configurations at every time $t \in \mathbb{R}$ are determined in the physical space $\tilde{\mathbb{R}}^3$ by deformations that are one-to-one, orientation preserving, differentiable maps:

$$(x,t) \longmapsto y := \tilde{y}(x,t) \in \tilde{\mathbb{R}}^3.$$

The displacement field $\tilde{u}$ is defined by

$$(x,t) \longmapsto u := \tilde{u}(x,t) = \tilde{y}(x,t) - \iota(x),$$

where $\iota : \mathbb{R}^3 \longrightarrow \tilde{\mathbb{R}}^3$ is the identification map between $\mathbb{R}^3$ and $\tilde{\mathbb{R}}^3$. The condition $||Du|| << 1$ at any x and t, where $||\cdot||$ is the Frobenius norm, characterizes the small strain setting to which we refer our analyses, so that we can avoid distinguishing between reference, $\mathcal{B}$, and current $\tilde{y}(\mathcal{B},t)$ configurations.

A differentiable vector field

$$(x,t) \longmapsto \nu(x,t) \in \hat{\mathbb{R}}^3$$

describes in time at every body point the phason degrees of freedom. We indicate by N the spatial derivative $D\nu$ evaluated at x and t; $\hat{\mathbb{R}}^3$ is also isomorphic to $\mathbb{R}^3$. However, the two spaces are considered to be distinguished as $\tilde{\mathbb{R}}^3$ and $\mathbb{R}^3$ (in essence, the three copies of the 3D real space are analogous to the choice of three different coordinate systems in the same space).

Remark 2.1. Looking at quasi-periodic (atomic) lattices as the projection of a periodic higher-dimensional lattice over an appropriate subspace implies considering the additional degrees of freedom revealed by the Fourier analysis as observable entities. An observer—we know—is defined by the assignment of frames of reference in all spaces adopted to describe the morphology of a body and its motion. In what we discuss here, these spaces are $\mathbb{R}^3$, $\tilde{\mathbb{R}}^3$, $\hat{\mathbb{R}}^3$ and the time scale. Consider two such observers, say $\mathcal{O}$ and $\mathcal{O}'$, and presume that they record the same reference space $\mathbb{R}^3$ and time scale while they are distinguished in the physical space $\tilde{\mathbb{R}}^3$ and phason space $\hat{\mathbb{R}}^3$ by rigid-body motions. Thus, if y is the current placement of a material element as recorded

by $\mathcal{O}$, the transition $\mathcal{O} \longrightarrow \mathcal{O}'$ implies

$$y \longmapsto y' = \mathfrak{w}(t) + Q(t)(y - y_0),$$

where y' is the placement recorded by $\mathcal{O}'$ while $\mathfrak{w}(t) \in \mathbb{R}^3$ and $Q(t) \in SO(3)$ depend smoothly on time and y_0 is a fixed point chosen arbitrarily. Consequently, u will change as $u \longmapsto u' = \mathfrak{w}(t) - \iota(x) + Q(t)(y - y_0)$ and the velocity $\dot{u} := \mathrm{d}\tilde{u}(x,t)/\mathrm{d}t$ as $\dot{u} \longmapsto \dot{u}' = \mathfrak{w}(t) + \dot{Q}(t)(y - y_0) + Q(t)\dot{u}$. Thus, the pull-back of $\dot{u}'$ into the frame of reference that defines $\mathcal{O}$ is

$$u^{\diamond} = Q^{\top}(t)\dot{u}' = \mathfrak{c}(t) + q(t) \times (y - y_0) + \dot{u},$$

where $\mathfrak{c}(t) := Q^{\top}(t)\mathfrak{w}(t)$ and $q(t)$ is the axial vector of the skew-symmetric tensor $Q^{\top}(t)\dot{Q}(t)$. Since the phason vector ν is insensitive to rigid relative translations of the observers, for reasons already recalled, in the phason space $\hat{\mathbb{R}}^3$ the transition $\mathcal{O} \longrightarrow \mathcal{O}'$ implies $\nu \longmapsto \nu' = Q(t)\nu$, so that the velocity $\dot{\nu} := \mathrm{d}\tilde{\nu}(x,t)/\mathrm{d}t$ changes as $\dot{\nu} \longmapsto \dot{\nu}' = \dot{Q}(t)\nu + Q(t)\dot{\nu}$. Its pull-back in the frame of reference that defines $\mathcal{O}$ leads to

$$\dot{\nu}^{\diamond} = Q^{\top}(t)\dot{\nu}' = q(t) \times \nu.$$

These relations are expressed in Lagrangian representation because this has been the above choice in defining motions. They have the obvious analogous counterparts in the Eulerian representation of the velocities.

(b) Interactions and their balance equations

Bulk and contact actions perform power in the displacement time rate. The former are subdivided into non-inertial ($\mathbf{b}$) and inertial ($\mathbf{b}^{in}$) components; the latter component is such that $\mathbf{b}^{in} = -\rho\ddot{u}$, where ρ is the density of mass, presumed here to be constant. Since we restrict our analysis to the small strain regime, we do not distinguish the reference configuration $\mathcal{B}$ from the current one, that is, $\tilde{y}(\mathcal{B}, t)$. Thus, we avoid distinguishing between the acceleration $\ddot{u}$ from its Eulerian counterpart and will continue to write x as a space variable. In this setting, the Cauchy stress tensor $\boldsymbol{\sigma}$ and the first Piola–Kirchhoff stress P coincide up to leading-order terms and the same holds for the relation between non-inertial bulk actions in Lagrangian and Eulerian representations.

Phason actions perform power in the time rate of ν. They are also distinguished into bulk and contact families. In the former class, we exclude external bulk actions because no external fields act directly on phasons and we record only three sound-like branches in experiments [32], so that we exclude phason inertia, while we include a phason self-action ($\boldsymbol{\zeta}$) that is not postulated; rather its existence is derived (see [11] for the proof). Contact phason actions are represented by a microstress ($\mathcal{S}$), also called phason stress. Pertinent balance equations are as follows:

$$\mathrm{div}\boldsymbol{\sigma} + \mathbf{b} = \rho\ddot{u},$$

$$\mathrm{div}\mathcal{S} = \boldsymbol{\zeta}$$

and

$$\mathrm{skew}(\boldsymbol{\sigma} + \nu \otimes \boldsymbol{\zeta} + \mathcal{S}^{\top}\nabla\nu) = 0,$$

where skew$(\cdot)$ indicates the skew-symmetric part of its argument.

Remark 2.2. The validity of the previous system of balance equations is based on a proof provided in [11] (see also [20,33]). We sketch here essential aspects of it. To this aim, it is expedient to make an excursion in the large strain regime. We refer to a reference configuration $\mathcal{B}$ that is a fit region in the standard sense. Then, we can pass to an exterior domain progressively enlarging $\mathcal{B}$ in a sequence and computing a limit in a procedure such that the results obtained hold at every step of the sequence. Take an arbitrary subset $\mathfrak{b}$ of $\mathcal{B}$ that is still, as $\mathcal{B}$, a bounded, open, connected set with surface-like boundary $\partial\mathfrak{b}$ oriented by the outward unit normal n to within a finite number

of corners and edges. Dividing as usual the external actions exerted on $\mathfrak{b}$ into bulk and contact families, their power $\mathcal{P}^{\text{ext}}_{\mathfrak{b}}$ is formally given by

$$\mathcal{P}^{\text{ext}}_{\mathfrak{b}}(\dot{u},\dot{\nu}) := \int_{\mathfrak{b}} (\mathbf{b}^{\ddagger}_{R}\cdot\dot{u} + \mathfrak{f}_{R}\cdot\dot{\nu})\,\mathrm{d}x + \int_{\partial\mathfrak{b}} (\mathfrak{t}_{\partial}\cdot\dot{u} + \boldsymbol{\tau}_{\partial}\cdot\dot{\nu})\,\mathrm{d}\mathcal{H}^{2}(x),$$

where $\mathrm{d}\mathcal{H}^{2}(x)$ is the area measure; the referential vector of body forces $\mathbf{b}^{\ddagger}_{R}$ is such that $\mathbf{b}^{\ddagger}_{R} = \mathbf{b} + \mathbf{b}^{in}$; $\mathfrak{f}_{R}$ is a formal external phason bulk action; $\mathfrak{t}_{\partial}$ is the standard traction and $\boldsymbol{\tau}_{\partial}$ is a phason contact action—the contact actions depend on x, t and the boundary $\partial\mathfrak{b}$, as indicated by the subscript ∂. We require objectivity of the external power. Formally, the requirement is $\mathcal{P}^{\text{ext}}_{\mathfrak{b}}(\dot{u},\dot{\nu}) = \mathcal{P}^{\text{ext}}_{\mathfrak{b}}(\dot{u}^{\diamond},\dot{\nu}^{\diamond})$ for any choice of $\mathfrak{b}$ and the vectors $\mathfrak{c}(t)$ and $q(t)$ in the expressions of $\dot{u}^{\diamond}$ and $\dot{\nu}^{\diamond}$ in remark 2.1. Integral balances of actions are immediate consequences; they are the standard integral balance of forces:

$$\int_{\mathfrak{b}} \mathbf{b}^{\ddagger}_{R}\,\mathrm{d}x + \int_{\partial\mathfrak{b}} \mathfrak{t}_{\partial}\,\mathrm{d}\mathcal{H}^{2}(x),$$

and a non-standard integral balance of couples:

$$\int_{\mathfrak{b}} ((y-y_{0})\times\mathbf{b}^{\ddagger}_{R} + \nu\times\mathfrak{f}_{R}\cdot\dot{\nu})\,\mathrm{d}x + \int_{\partial\mathfrak{b}} ((y-y_{0})\times\mathfrak{t}_{\partial} + \nu\times\boldsymbol{\tau}_{\partial})\,\mathrm{d}\mathcal{H}^{2}(x).$$

Common assumptions of boundedness of $||\mathbf{b}^{\ddagger}_{R}||$ and regularity of $\mathfrak{t}_{\partial}(\cdot,t)$ imply the Cauchy theorem, that is, the validity of the relations $\mathfrak{t}_{\partial}(x,t) = \mathfrak{t}(x,t,n) = -\mathfrak{t}(x,t,-n) = P(x,t)n$, where P is, as already mentioned, the first Piola–Kirchhoff stress. When $P(\cdot,t)$ is $C^{1}(\mathcal{B})\cap C(\bar{\mathcal{B}})$, the overbar denoting set closure, the local balance of forces in terms of P follows. Also, since $\mathcal{B}$ is bounded, we can choose y_{0} in a way such that the boundedness of $||\mathbf{b}^{\ddagger}_{R}||$ implies the one of $||(y-y_{0})\times\mathbf{b}^{\ddagger}_{R}||$. Then, assuming that $||\mathfrak{f}^{\ddagger}_{R}||$ is also bounded, with regularity assumptions on $\boldsymbol{\tau}_{\partial}(\cdot,t)$ analogous to those for $\mathfrak{t}_{\partial}(\cdot,t)$, a Cauchy theorem for $\boldsymbol{\tau}_{\partial}$ holds and leads to the existence of a microstress $\mathcal{S}_{R}$ such that $\boldsymbol{\tau}_{\partial}(x,t) = \boldsymbol{\tau}(x,t,n) = -\boldsymbol{\tau}(x,t,-n) = \mathcal{S}_{R}(x,t)n$. When $\mathcal{S}_{R}(\cdot,t)\in C^{1}(\mathcal{B})\cap C(\bar{\mathcal{B}})$ at every t, there exists $\mathfrak{z}$ such that for $F := \nabla u + I$, with I the second-rank unit tensor (a shifter between the reference and current spaces) and $\det F > 0$, we have

$$\mathrm{div}\mathcal{S}_{R} - \mathfrak{z} + \mathfrak{f}^{\ddagger}_{R} = 0 \quad \text{and} \quad \mathrm{skew}(PF^{\top} + \nu\otimes\mathfrak{z} + \mathcal{S}^{\top}_{R}\nabla\nu).$$

As already mentioned, we set $\mathfrak{f}_{R} = 0$ because we have no evidence of external bulk direct actions on the phason field, including inertial effects. The Eulerian counterparts of the remaining actions in the above relations are

$$\boldsymbol{\sigma} = (\det F)^{-1}PF^{\top}, \quad \boldsymbol{\zeta} = (\det F)^{-1}\mathfrak{z}, \quad \mathcal{S} = (\det F)^{-1}\mathcal{S}_{R}F^{\top}.$$

Remark 2.3. Before the formal proof of existence in [11], the phason self-action was postulated in [34] but only with dissipative nature, which leads to diffusion. Later, after the formal existence proof, which is independent of constitutive choices, it does not exclude the possible presence of a conservative component, and the phason self-action has been accepted [35] with its structure potentially involving both conservative and dissipative components.

(c) Constitutive structures

As already mentioned, our analysis remains confined to the linearized elastic setting. Thus, we attribute to $\boldsymbol{\sigma}$, $\mathcal{S}$ and $\boldsymbol{\zeta}$ only conservative nature and they are presumed to be given by an energy of the type $e = \tilde{e}(x,\nabla u,\nu,\nabla\nu)$, so that [10,11]

$$\boldsymbol{\sigma} = \frac{\partial e}{\partial\nabla u}, \qquad \mathcal{S} = \frac{\partial e}{\partial\nabla\nu}, \qquad \boldsymbol{\zeta} = \frac{\partial e}{\partial\nu}. \tag{2.1}$$

In a small strain regime, the one considered here, we can assume a quadratic form for the energy, that is,

$$e(x,\nabla u,\nu,\nabla\nu) = \frac{1}{2}(\mathbb{C}(x)\nabla u)\cdot\nabla u + \frac{1}{2}(\mathbb{K}(x)\nabla\nu)\cdot\nabla\nu + (\mathbb{K}(x)'\nabla\nu)\cdot\nabla u + \frac{1}{2}a|\nu|^{2},$$

where $\mathbb{C}$, $\mathbb{K}$ and $\mathbb{K}'$ are fourth-rank constitutive tensors and a is a positive constant; $\mathbb{C}$ is the standard elastic tensor with major and minor symmetries; $\mathbb{K}'$ describes the coupling between gross deformation and phason field; $\mathbb{K}$ is peculiar of the phason degrees of freedom. These constitutive tensors are constant in each half-plane considered; the constant values in the two half-planes are different. Appropriate explicit structures of the constitutive tensors are given in [6,11,36].

Remark 2.4. Another excursion in the large strain regime further clarifies the presence of ν in the list of entries of $\tilde{e}(\cdot)$. Consider an elastic energy density of the type

$$e = \tilde{e}(u, F, \nu, \nabla\nu).$$

Physics requires that e be objective, that is, the elastic energy density is insensitive to rigid-body type changes of observers. According to the relations in remark 2.1, objectivity requires

$$\tilde{e}(u, F, \nu, \nabla\nu) = \tilde{e}(\bar{\mathfrak{w}} + Q(y - y_0), F, Q\nu, Q\nabla\nu)$$

for every $Q \in SO(3)$ and $\bar{\mathfrak{w}} := \mathfrak{w}(t) - \iota(x)$. The arbitrariness of $\bar{\mathfrak{w}}$ implies that $\hat{e}(\cdot)$ cannot depend on u, while it can depend on ν. Structures of the form

$$\tilde{e}(F^\top F, |\nu|, (\nabla\nu)^\top \nabla\nu) \quad \text{or} \quad \tilde{e}(F^\top F, F^{-1}\nu, F^{-1}\nabla\nu)$$

are objective. Other choices are available.

(d) Two-dimensional ambient setting

We reduce our analyses to the 2D ambient setting. We thus consider the explicit expressions of the constitutive tensors given in [36]. They are as follows:

$$\mathbb{C}_{ijkl} = \lambda\delta_{ij}\delta_{kl} + \mu(\delta_{ik}\delta_{jl} + \delta_{il}\delta_{jk}),$$

$$\mathbb{K}_{ijkl} = k_1\delta_{ik}\delta_{jl} + k_2(\delta_{ij}\delta_{kl} - \delta_{il}\delta_{jk})$$

and

$$\mathbb{K}'_{ijkl} = k_3(\delta_{i1} - \delta_{i2})(\delta_{ij}\delta_{kl} - \delta_{ik}\delta_{jl} + \delta_{il}\delta_{jk}).$$

The indices take values 1 and 2. No summation over repeated indices is assumed in the last equation; λ and μ are the standard Lamé constants; k_1 and k_2 are associated only with the inhomogeneity of ν, that is, with $\nabla\nu$; k_3 is a *coupling coefficient*.

We presume that $\tilde{e}(\cdot)$ is non-negative for any choice of ∇u and $\nabla\nu$, with $e = 0$ only for rigid rotations. These conditions lead to the following limitations for the elastic constants:

$$\lambda + \mu > 0, \quad k_1 > k_2, \quad k_1 + k_2 + 2\mu > \sqrt{(k_1 + k_2 - 2\mu)^2 + (4k_3)^2}.$$

3. Analysis in the absence of phason self-action

For simplicity, in what follows, we exclude external non-inertial bulk actions; that is, we set $\mathbf{b} = 0$.

First, we consider the case in which $\boldsymbol{\zeta} = 0$. Under this condition, the model structure reduces to a higher-dimensional version of the traditional linearized elasticity of simple bodies. Thus, we are able to provide a closed-form solution that can be adopted as a benchmark in more articulated numerical analyses.

(a) A formulation based on the Stroh formalism

In the plane, we fix a reference frame Ox_1x_2. Set

$$\mathfrak{u} := (u_1, u_2, v_1, v_2).$$

During steady-state crack propagation along the x_1-axis, the second time derivative of $\mathfrak{u}$ can be expressed as

$$\ddot{\mathfrak{u}} = c^2\mathfrak{u}_{,11},$$

where c is the *propagation speed* and the comma denotes differentiation with respect to the space components indicated by the indices after the comma itself.

Set also

$$\mathsf{s} := (\sigma_{11}, \sigma_{21}, \mathcal{S}_{11}, \mathcal{S}_{21}) \quad \text{and} \quad \mathsf{t} := (\sigma_{12}, \sigma_{22}, \mathcal{S}_{12}, \mathcal{S}_{22}).$$

The constitutive relations can be rewritten as

$$\begin{pmatrix} \mathsf{s} \\ \mathsf{t} \end{pmatrix} = \begin{bmatrix} \mathsf{Q} & \mathsf{R} \\ \mathsf{R}^T & \mathsf{T} \end{bmatrix} \begin{pmatrix} \mathsf{u}_{,1} \\ \mathsf{u}_{,2} \end{pmatrix},$$

where

$$\mathsf{Q} = \begin{bmatrix} 2\mu+\lambda & 0 & k_3 & 0 \\ 0 & \mu & 0 & k_3 \\ k_3 & 0 & k_1 & 0 \\ 0 & k_3 & 0 & k_1 \end{bmatrix}, \quad \mathsf{R} = \begin{bmatrix} 0 & \lambda & 0 & k_3 \\ \mu & 0 & -k_3 & 0 \\ 0 & -k_3 & 0 & k_2 \\ k_3 & 0 & -k_2 & 0 \end{bmatrix}$$

and

$$\mathsf{T} = \begin{bmatrix} \mu & 0 & -k_3 & 0 \\ 0 & 2\mu+\lambda & 0 & -k_3 \\ -k_3 & 0 & k_1 & 0 \\ 0 & -k_3 & 0 & k_1 \end{bmatrix}.$$

Thus, under steady-state conditions, the balance equation is

$$\mathsf{s}_{,1} + \mathsf{t}_{,2} = \rho c^2 \mathsf{D}\mathsf{u}_{,11},$$

where $\mathsf{D} = \mathrm{diag}(1,1,0,0)$. Equivalently, we can write

$$\begin{pmatrix} \mathsf{u}_{,1} \\ \mathsf{u}_{,2} \end{pmatrix}_{,1} + \begin{bmatrix} \mathsf{Q}_0^{-1}(\mathsf{R}+\mathsf{R}^\top) & \mathsf{Q}_0^{-1}\mathsf{T} \\ -\mathsf{I} & 0 \end{bmatrix} \begin{pmatrix} \mathsf{u}_{,1} \\ \mathsf{u}_{,2} \end{pmatrix}_{,2} = \begin{pmatrix} 0 \\ 0 \end{pmatrix}, \tag{3.1}$$

where I is the identity in $\mathbb{M}_{4\times4}$, the space of 4×4 real matrices, and $\mathsf{Q}_0 = \mathsf{Q} - \rho c^2 \mathsf{D}$. The properties of the 8×8 coefficient matrix in equation (3.1) have been analysed in [28]. We adopt a change of variable $\mathsf{u} \longrightarrow \mathsf{g}$ provided by the generalized eigenvectors of this matrix and given by

$$\begin{pmatrix} \mathsf{u}_{,1} \\ \mathsf{u}_{,2} \end{pmatrix} = \begin{bmatrix} \mathsf{E} & \bar{\mathsf{E}} \\ \mathsf{F} & \bar{\mathsf{F}} \end{bmatrix} \begin{pmatrix} \mathsf{g} \\ \bar{\mathsf{g}} \end{pmatrix} = 2\mathrm{Re} \begin{pmatrix} \mathsf{E}\mathsf{g} \\ \mathsf{F}\mathsf{g} \end{pmatrix}, \tag{3.2}$$

where the overbar denotes complex conjugation, g is a four-dimensional vector,

$$\mathsf{E} := \begin{bmatrix} \dfrac{m_1^2}{\sqrt{1-m_1^2}} & m_2^2 & 0 & -i\dfrac{2(\lambda+\mu)+\rho v^2}{4\chi(\lambda+\mu)} \\ im_1^2 & i\dfrac{m_2^2}{\sqrt{1-m_2^2}} & 0 & \dfrac{2(\lambda+\mu)-\rho v^2}{4\chi(\lambda+\mu)} \\ -\chi\dfrac{4-3m_1^2}{\sqrt{1-m_1^2}} & -\chi(4-m_2^2) & -1 & i(1-\dfrac{(\rho v^2)^2}{8\chi k_3(\lambda+\mu)}) \\ -i\chi(4-m_1^2) & -i\chi\dfrac{4-3m_2^2}{\sqrt{1-m_2^2}} & -i & -1 \end{bmatrix}$$

and

$$\mathsf{F} := \begin{bmatrix} im_1^2 & im_2^2\sqrt{1-m_2^2} & 0 & \dfrac{2(\lambda+\mu)+\rho v^2}{4\chi(\lambda+\mu)} \\ -m_1^2\sqrt{1-m_1^2} & -m_2^2 & 0 & i\dfrac{2(\lambda+\mu)-\rho v^2}{4\chi(\lambda+\mu)} \\ -i\chi(4-3m_1^2) & -i\chi(4-m_2^2)\sqrt{1-m_2^2} & -i & \dfrac{(\rho v^2)^2}{8\chi k_3(\lambda+\mu)} \\ \chi(4-m_1^2)\sqrt{1-m_1^2} & \chi(4-3m_2^2) & 1 & 0 \end{bmatrix},$$

with i the imaginary unit and

$$\chi = \frac{k_3}{k_1}.$$

The scalars

$$m_1^2 = \frac{\rho c^2}{2\mu + \lambda - \chi k_3} = \frac{c^2}{c_L^2} \quad \text{and} \quad m_2^2 = \frac{\rho c^2}{\mu - \chi k_3} = \frac{c^2}{c_S^2}$$

are the Mach numbers, with c_L and c_S the longitudinal and shear wave speeds, respectively. We consider only subsonic crack propagation occurring for values of the crack-tip speed c smaller than the lower wave speed of the two materials.

Owing to the structure of $\mathtt{E}$ and $\mathtt{F}$, we have

$$\begin{bmatrix} \mathtt{Q}_0^{-1}(\mathtt{R}+\mathtt{R}^T) & \mathtt{Q}^{-1}\mathtt{T} \\ -\mathtt{I} & 0 \end{bmatrix} \begin{bmatrix} \mathtt{E} & \bar{\mathtt{E}} \\ \mathtt{F} & \bar{\mathtt{F}} \end{bmatrix} = \begin{bmatrix} \mathtt{E} & \bar{\mathtt{E}} \\ \mathtt{F} & \bar{\mathtt{F}} \end{bmatrix} \begin{bmatrix} \mathtt{W}+\mathtt{N} & 0 \\ 0 & \overline{\mathtt{W}}+\mathtt{N} \end{bmatrix},$$

where $\mathtt{N}$ is the nilpotent matrix

$$\mathtt{N} := \begin{bmatrix} 0 & 0 & 0 & 0 \\ 0 & 0 & 0 & 0 \\ 0 & 0 & 0 & 1 \\ 0 & 0 & 0 & 0 \end{bmatrix} \tag{3.3}$$

and

$$\mathtt{W} = \mathrm{diag}(\omega_1, \omega_2, \omega_3, \omega_3),$$

with

$$\omega_1 = \frac{i}{\sqrt{1-m_1^2}}, \quad \omega_2 = \frac{i}{\sqrt{1-m_2^2}}, \quad \omega_3 = i,$$

and $\mathtt{N}^2 = 0$. Inserting equation (3.2) into equation (3.1), we obtain

$$\mathtt{g}_{,1} + (\mathtt{W}+\mathtt{N})\mathtt{g}_{,2} = 0, \tag{3.4}$$

and its complex conjugate. A general solution to the differential system equation (3.4) has the form

$$\mathtt{g} = \mathtt{q}(z) - \frac{i}{2}\bar{z}\mathtt{N}\mathtt{q}'(z), \tag{3.5}$$

where the prime indicates differentiation with respect to the argument of the function considered, and $\mathtt{q}(z)$ is a four-dimensional vector with components $\mathtt{q}_k(z_k)$, where

$$z_k = x_1 + ix_2\sqrt{1-m_k^2}, \quad k = 1,2,3,4,$$

with $m_3 = m_4 = 0$, so that $z_3 = z_4 = x_1 + ix_2$. Once $\mathtt{q}$ and $\mathtt{g}$ have been determined, by considering the boundary conditions of the specific problem at hands, we get

$$\mathtt{u}_{,1} = 2\mathrm{Re}[\mathtt{E}\mathtt{g}] \quad \text{and} \quad \mathtt{t} = 2\mathrm{Re}[\mathtt{H}\mathtt{g}],$$

where

$$\mathtt{H} = \mathtt{R}^T\mathtt{E} + \mathtt{T}\mathtt{F}.$$

(b) An interface crack between two different quasicrystals

Consider two distinct planar quasi-crystalline materials joined along a straight line that we identify with the x_1-axis, indicated below simply by x for conciseness because x_2 does not explicitly enter into the derived expressions. The origin of the coordinate system is placed at the crack tip (figure 2).

The index $l = \mathrm{I}, \mathrm{II}$ distinguishes the two quasicrystals in the following analyses. We choose $l = \mathrm{I}$ to indicate the upper half-plane, while $l = \mathrm{II}$ refers to the lower half-plane.

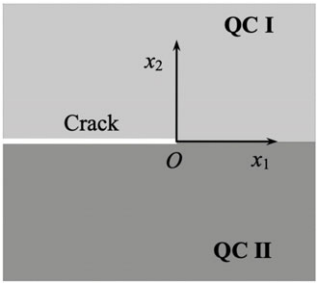

Figure 2. Geometry of the problem considered.

We indicate by f_l the analytic vector function

$$\mathsf{f}_l = \mathsf{q}_l(z) - \frac{i}{2} z \mathsf{N} \mathsf{q}_l'(z), \tag{3.6}$$

which coincides with $\mathsf{g}_l = \mathsf{h}_l(z) - \frac{i}{2}\bar{z}\mathsf{N}\mathsf{h}_l'(z)$, for $\mathrm{Im}[z] = 0$. Then, we have

$$\mathsf{u}_l' = \mathsf{E}_l \mathsf{f}_l(x) + \bar{\mathsf{E}}_l \bar{\mathsf{f}}_l(x) \tag{3.7}$$

and

$$\mathsf{t}_l = \mathsf{H}_l \mathsf{f}_l(x) + \bar{\mathsf{H}}_l \bar{\mathsf{f}}_l(x), \tag{3.8}$$

with x real; from now on, we simply write x instead of x_1 for conciseness.

At the interface, we have

$$\mathsf{u}_{\mathrm{I}}'(x) = \mathsf{u}_{\mathrm{II}}'(x), \quad \mathsf{t}_{\mathrm{I}}(x) = \mathsf{t}_{\mathrm{II}}(x), \quad \text{for } x > 0 \tag{3.9}$$

and

$$\mathsf{t}_{\mathrm{I}}(x) = \mathsf{t}_{\mathrm{II}}(x) = 0, \quad \text{for } x < 0. \tag{3.10}$$

Using equation (3.8), the stress continuity at the interface also reads as

$$\mathsf{H}_{\mathrm{I}} \mathsf{f}_{\mathrm{I}}(x) - \bar{\mathsf{H}}_{\mathrm{II}} \bar{\mathsf{f}}_{\mathrm{II}}(x) = \mathsf{H}_{\mathrm{II}} \mathsf{f}_{\mathrm{II}}(x) - \bar{\mathsf{H}}_{\mathrm{I}} \bar{\mathsf{f}}_{\mathrm{I}}(x). \tag{3.11}$$

Thus, both sides of equation (3.11) must coincide with the same entire function, say p, depending on z, such that

$$\bar{\mathsf{f}}_{\mathrm{II}}(z) = \bar{\mathsf{H}}_{\mathrm{II}}^{-1}(\mathsf{H}_{\mathrm{I}} \mathsf{f}_{\mathrm{I}}(z) - \mathsf{p}(z)) \quad \text{and} \quad \bar{\mathsf{f}}_{\mathrm{I}}(z) = \bar{\mathsf{H}}_{\mathrm{I}}^{-1}(\mathsf{H}_{\mathrm{II}} \mathsf{f}_{\mathrm{II}}(z) - \mathsf{p}(z)). \tag{3.12}$$

Since the tractions are assumed to be finite at large distance from the crack tip, the functions f_{I} and f_{II} must be bounded as $|z| \longrightarrow +\infty$. Thus, the function p must be constant by the Liouville theorem and we indicate the constant value again with p.

Let d be the jump of u at the interface, defined by

$$\mathsf{d}(x) := \mathsf{u}^+(x) - \mathsf{u}^-(x),$$

where u^+ and u^- are the upper and lower limits of u at the interface. We have

$$\mathsf{d}'(x) = \left(\mathsf{E}_{\mathrm{I}} \mathsf{H}_{\mathrm{I}}^{-1} - \bar{\mathsf{E}}_{\mathrm{II}} \bar{\mathsf{H}}_{\mathrm{II}}^{-1}\right) \mathsf{H}_{\mathrm{I}} \mathsf{f}_{\mathrm{I}}(x) - \left(\mathsf{E}_{\mathrm{II}} \mathsf{H}_{\mathrm{II}}^{-1} - \bar{\mathsf{E}}_{\mathrm{I}} \bar{\mathsf{H}}_{\mathrm{I}}^{-1}\right) \mathsf{H}_{\mathrm{II}} \mathsf{f}_{\mathrm{II}}(x) - \left(\bar{\mathsf{E}}_{\mathrm{I}} \bar{\mathsf{H}}_{\mathrm{I}}^{-1} - \bar{\mathsf{E}}_{\mathrm{II}} \bar{\mathsf{H}}_{\mathrm{II}}^{-1}\right) \mathsf{p}. \tag{3.13}$$

Set $\mathsf{Y}_{\mathrm{I}} := i \mathsf{E}_{\mathrm{I}} \mathsf{H}_{\mathrm{I}}^{-1}$ and $\mathsf{Y}_{\mathrm{II}} := i \mathsf{E}_{\mathrm{II}} \mathsf{H}_{\mathrm{II}}^{-1}$. We define Z as

$$Z := \mathsf{Y}_{\mathrm{I}} + \bar{\mathsf{Y}}_{\mathrm{II}}.$$

The matrices Y_{I}, Y_{II} and Z are Hermitian for subsonic crack-tip speed, as shown in [28], so that $\bar{Z} = Z^\top$. Thus, the expression equation (3.13) can be rewritten as

$$i\mathsf{d}'(x) = Z \mathsf{H}_{\mathrm{I}} \mathsf{f}_{\mathrm{I}}(x) - \bar{Z} \mathsf{H}_{\mathrm{II}} \mathsf{f}_{\mathrm{II}}(x) + (\bar{\mathsf{Y}}_{\mathrm{I}} + \bar{\mathsf{Y}}_{\mathrm{II}})\mathsf{p}. \tag{3.14}$$

The interface condition equation (3.9)$_1$ implies $\mathsf{d}'(x) = 0$ for $x > 0$; so, from equation (3.14), always for $x > 0$, we get

$$Z\mathsf{H}_{\mathrm{I}}\mathsf{f}_{\mathrm{I}}(x) = \bar{Z}\mathsf{H}_{\mathrm{II}}\mathsf{f}_{\mathrm{II}}(x) + (\overline{\mathsf{Y}}_{\mathrm{I}} + \overline{\mathsf{Y}}_{\mathrm{II}})\mathsf{p}.$$

Thus, we can introduce an analytic vector function h supported on the whole complex plane but the crack ($\mathrm{Im}[z] = 0$ and $\mathrm{Re}[z] < 0$) and defined by

$$\mathsf{h}(z) = \begin{cases} \mathsf{H}_{\mathrm{I}}\mathsf{f}_{\mathrm{I}}(z), & \text{for } \mathrm{Im}[z] > 0, \\ Z^{-1}(\bar{Z}\mathsf{H}_{\mathrm{II}}\mathsf{f}_{\mathrm{II}}(z) + (\overline{\mathsf{Y}}_{\mathrm{II}} - \overline{\mathsf{Y}}_{\mathrm{I}})\mathsf{p}), & \text{for } \mathrm{Im}[z] < 0. \end{cases} \tag{3.15}$$

Using equations (3.12) and (3.15), from equation (3.8) we obtain

$$\mathsf{t}_{\mathrm{I}}(x) = \mathsf{h}^{+}(x) + \bar{Z}^{-1}(Z\mathsf{h}^{-}(x) - (\mathsf{Y}_{\mathrm{II}} + \overline{\mathsf{Y}}_{\mathrm{II}})\mathsf{p}), \tag{3.16}$$

where the superscript '+' denotes the restriction of h to the half-plane $\mathrm{Im}[z] > 0$, and the superscript '−' refers to the lower half-plane. Moreover, equation (3.14) becomes

$$i\mathsf{d}'(x) = Z[\mathsf{h}^{+} - \mathsf{h}^{-}](x).$$

In terms of h, the traction free condition along the crack margins reads

$$\bar{Z}\mathsf{h}^{+}(x) + Z\mathsf{h}^{-}(x) = (\mathsf{Y}_{\mathrm{II}} + \overline{\mathsf{Y}}_{\mathrm{II}})\mathsf{p}, \quad \text{for } x < 0. \tag{3.17}$$

So, h satisfies a Riemann–Hilbert problem. A special solution is

$$\mathsf{h}(z) = (Z + \bar{Z})^{-1}(\mathsf{Y}_{\mathrm{II}} + \overline{\mathsf{Y}}_{\mathrm{II}})\mathsf{p}.$$

In particular, we presume for h the following structure:

$$\mathsf{h}(z) = z^{\alpha}\mathsf{w},$$

where w is a constant four-dimensional vector and α is a complex number with

$$-1 < \mathrm{Re}[\alpha] \leq 0.$$

Both w and α need to be determined. Therefore, the assumed expression for $\mathsf{h}(z)$ admits the following limits in both sides of the negative real axis, that is, for $z = -x\exp(\pm i\pi)$:

$$\mathsf{h}^{\pm}(x) = (-x)^{\alpha}\exp(\pm i\pi\alpha)\mathsf{w}, \qquad \text{for } x < 0.$$

Insertion of such an expression into equation (3.17) yields

$$(\bar{Z} + \exp(-i2\pi\alpha)Z)\mathsf{w} = 0, \tag{3.18}$$

which is an eigenvalue problem. For subsonic crack-tip speed, the matrix Z is Hermitian, as proven in [28]. Thus, it can be written as

$$Z = \mathrm{D} + i\mathrm{W},$$

where D is symmetric and W is skew-symmetric; both matrices have real entries. Then, equation (3.18) becomes

$$(\mathrm{D}^{-1}\mathrm{W} + i\beta\mathsf{I})\mathsf{w} = 0,$$

where I has been already introduced and

$$\beta = -i\cot\pi\alpha. \tag{3.19}$$

In particular, since W is of even order and skew-symmetric, we have $\det\mathrm{W} \geq 0$. In the specific case considered here, we also have $\det\mathrm{W} \ll 1$. The eigenvalues β are roots of the characteristic

equation

$$\det(\mathrm{D}^{-1}\mathrm{W} + i\beta\mathrm{I}) = 0,$$

that is,

$$\beta^4 - 2b\beta^2 + c = 0, \tag{3.20}$$

with

$$b := -\frac{1}{4}\mathrm{tr}\left(\left(\mathrm{W}\mathrm{D}^{-1}\right)^2\right) \quad \text{and} \quad c := \frac{\det \mathrm{W}}{\det \mathrm{D}}.$$

Thus, if D is positive definite, owing to the already recalled properties of W, we have $b \geq 0$. The roots of equation (3.20) are thus

$$\beta_1 = -\sqrt{b - \sqrt{b^2 - c}}, \qquad \beta_2 = -\sqrt{b + \sqrt{b^2 - c}}$$

and

$$\beta_3 = -\beta_1, \quad \beta_4 = -\beta_2.$$

For subsonic crack propagation, we have $0 < c < b$, so that $0 < |\beta_k| < 1$, $k = 1, 2, 3, 4$. Also, since $-1 < \mathrm{Re}[\alpha_k] \leq 0$, from equation (3.19) we obtain

$$\alpha_k = -\frac{1}{2\pi i}\ln\frac{\beta_k - 1}{\beta_k + 1}, \quad k = 1, 2, 3, 4.$$

The α_ks are complex conjugate, that is, $\alpha_3 = \bar{\alpha}_1$ and $\alpha_4 = \bar{\alpha}_2$. Since in the considered conditions $0 < |\beta_k| < 1$, as recalled above, we find

$$\alpha_1 = -\frac{1}{2} + i\gamma_1 \quad \text{and} \quad \alpha_2 = -\frac{1}{2} + i\gamma_2, \tag{3.21}$$

where

$$\gamma_1 = \frac{1}{2\pi}\ln\frac{1 + \sqrt{b - \sqrt{b^2 - c}}}{1 - \sqrt{b - \sqrt{b^2 - c}}} \quad \text{and} \quad \gamma_2 = \frac{1}{2\pi}\ln\frac{1 + \sqrt{b + \sqrt{b^2 - c}}}{1 - \sqrt{b + \sqrt{b^2 - c}}}$$

are real positive numbers: they are the oscillation indices of the displacement and phason fields. The corresponding eigenvectors are complex conjugate pairs: if $\mathtt{w}_1$ and $\mathtt{w}_2$ correspond to α_1 and α_2, their conjugate counterparts $\bar{\mathtt{w}}_1$ and $\bar{\mathtt{w}}_2$ are determined by $\alpha_3 = \bar{\alpha}_1$ and $\alpha_4 = \bar{\alpha}_2$, respectively. Then, from equations (3.18) and (3.21), we obtain

$$\bar{Z}\mathtt{w}_i = \exp(2\pi\gamma_i)Z\mathtt{w}_i \quad \text{and} \quad \bar{Z}\bar{\mathtt{w}}_i = \exp(-2\pi\gamma_i)Z\bar{\mathtt{w}}_i, \quad i = 1, 2.$$

Equation (3.18) and the Hermitian character of the matrix Z imply that the eigenvectors must satisfy the orthogonality conditions

$$\mathtt{w}_j \cdot Z\mathtt{w}_k = \mathtt{w}_j \cdot \bar{Z}\mathtt{w}_k = \bar{\mathtt{w}}_j \cdot Z\bar{\mathtt{w}}_k = \bar{\mathtt{w}}_j \cdot \bar{Z}\bar{\mathtt{w}}_k = 0, \quad \text{for } \mathrm{Im}[\alpha_i] \neq 0, \quad i, k = 1, 2, \tag{3.22}$$

and

$$\bar{\mathtt{w}}_j \cdot Z\mathtt{w}_k = \mathtt{w}_j \cdot Z\bar{\mathtt{w}}_k = \mathtt{w}_j \cdot \bar{Z}\bar{\mathtt{w}}_k = \bar{\mathtt{w}}_j \cdot \bar{Z}\mathtt{w}_k = 0, \quad \text{for } i \neq k, \quad j, k = 1, 2. \tag{3.23}$$

Then, the singular solution of the Riemann–Hilbert problem equation (3.18) is

$$\mathtt{h}(z) = \sum_{k=1}^{2}(r_k z^{\alpha_k}\mathtt{w}_k + s_k z^{\bar{\alpha}_k}\bar{\mathtt{w}}_k) + \mathrm{D}^{-1}\mathrm{Re}(\Upsilon_{\mathrm{II}})\mathtt{p}, \tag{3.24}$$

where r_k and s_k are undetermined complex constants. Since the traction $\mathtt{t}_{\mathrm{I}}(x)$ in equation (3.16) must be real along the interface at $x > 0$, as stated previously, we have

$$\mathtt{t}_{\mathrm{I}}(x) = \sum_{k=1}^{2}(r_k x^{\alpha_k}(1 - \exp(-i2\pi\alpha_k))\mathtt{w}_k + \bar{r}_k x^{\bar{\alpha}_k}(1 - \exp(-i2\pi\bar{\alpha}_k))\bar{\mathtt{w}}_k) \tag{3.25}$$

and

$$s_k = -\exp(-i2\pi\bar{\alpha}_k)\bar{r}_k, \quad i = 1, 2.$$

Notice that the vector $\mathtt{p}$ does not affect the expression of $\mathtt{t}_{\mathrm{I}}$.

On the basis of an analysis of interfacial cracks in simple elastic materials, as discussed in [37,38], we consider two complex stress intensity factors, $K_1 = K_{\rm II} + iK_{\rm I}$ and $K_2 = T_{\rm II} + iT_{\rm I}$, where $K_{\rm I}$ and $K_{\rm II}$ are the stress intensity factors of the standard stress $\boldsymbol{\sigma}$ while $T_{\rm I}$ and $T_{\rm II}$ are those of the phason stress $\mathcal{S}$. The factors K_1 and K_2 are such that

$$r_k = \frac{K_k}{(1-\exp(i2\pi\alpha_k))\sqrt{2\pi}}, \quad k = 1, 2.$$

Thus, from equation (3.24) we get

$$\mathtt{h}(z) = \frac{1}{\sqrt{2\pi}} \sum_{k=1}^{2} \left(\frac{K_k z^{\alpha_k}}{1-\exp(i2\pi\alpha_k)} \mathtt{w}_k + \frac{\bar{K}_k z^{\bar{\alpha}_k}}{1-\exp(i2\pi\bar{\alpha}_k)} \bar{\mathtt{w}}_k \right) + \mathtt{D}^{-1}\mathrm{Re}[\Upsilon_{\rm II}]\mathtt{p}. \tag{3.26}$$

The vector $\mathtt{t}_{\rm I}$ can be thus written as

$$\mathtt{t}_{\rm I}(x) = \frac{1}{\sqrt{2\pi}} \sum_{k=1}^{2} (K_k x^{\alpha_k} \mathtt{w}_k + \bar{K}_k x^{\bar{\alpha}_k} \bar{\mathtt{w}}_k) = \frac{1}{\sqrt{2\pi}} \sum_{k=1}^{2} (K_k x^{i\gamma_k} \mathtt{w}_k + \bar{K}_k x^{-i\gamma_k} \bar{\mathtt{w}}_k), \tag{3.27}$$

for $x > 0$, and we also have

$$\begin{aligned} \mathtt{d}'(x) &= \frac{1}{\sqrt{2\pi}} \sum_{k=1}^{2} ((-x)^{\alpha_k} i \exp(-i\pi\alpha_k) K_k \mathtt{Z}\mathtt{w}_k + (-x)^{\bar{\alpha}_k} i \exp(-i\pi\bar{\alpha}_k) \bar{K}_k \bar{\mathtt{Z}}\bar{\mathtt{w}}_k) \\ &= \frac{-1}{\sqrt{-2\pi x}} \sum_{k=1}^{2} ((-x)^{i\gamma_k} \exp(\pi\gamma_k) K_k \mathtt{Z}\mathtt{w}_k + (-x)^{\gamma_k} \exp(-\pi\gamma_k) \bar{K}_k \bar{\mathtt{Z}}\bar{\mathtt{w}}_k), \end{aligned} \tag{3.28}$$

for $x < 0$. Both standard (phonon) and phason stresses display square-root singularity and oscillatory behaviour in front of the crack tip, unless both γ_1 and γ_2 are vanishing small.

By integrating $\mathtt{d}'(x)$, we obtain

$$\mathtt{d}(x) = (\mathtt{Z} + \bar{\mathtt{Z}}) \sqrt{\frac{-x}{2\pi}} \sum_{k=1}^{2} \left(\frac{(-x)^{i\gamma_k} K_k \mathtt{w}_k}{(1+2i\gamma_k)\cosh\pi\gamma_k} + \frac{(-x)^{-i\gamma_k} \bar{K}_k \bar{\mathtt{w}}_k}{(1-2i\gamma_k)\cosh\pi\gamma_k} \right), \tag{3.29}$$

for $x < 0$. Moreover, since $\mathtt{N}^2 = 0$, from equations (3.6), (3.15) and (3.3) we obtain a representation vector $\mathtt{g}$ introduced in equation (3.5), given by

$$\mathtt{g}_l(z) = \mathtt{f}_l(z) + \frac{i}{2}(z - \bar{z})\,\mathtt{N}\mathtt{f}_l'(z), \quad l = \mathrm{I}, \mathrm{II}, \tag{3.30}$$

where

$$\mathtt{f}_{\rm I}(z) = \mathtt{H}_{\rm I}^{-1}\mathtt{h}(z) \quad \text{and} \quad \mathtt{f}_{\rm II}(z) = \mathtt{H}_{\rm II}^{-1}\bar{\mathtt{Z}}^{-1}\mathtt{Z}\mathtt{h}(z). \tag{3.31}$$

Introduction of equation (3.30) into equation (3.2) furnishes the expression of u and v over the whole plane.

(c) Energy release rate

We adopt an expression for the *energy release rate* $\mathcal{G}$ that is a direct extension to the description of quasicrystals of the one proposed in [39]. It is given by

$$\mathcal{G} := \lim_{\hat{\lambda} \longrightarrow 0} \frac{1}{2\hat{\lambda}} \int_0^{\hat{\lambda}} \mathtt{t}(\hat{\lambda} - \varsigma) \cdot \mathtt{d}(-\varsigma)\, \mathrm{d}\varsigma,$$

where $\hat{\lambda}$ is an arbitrary length scale. At first glance, one could believe that the reason of our choice is that, in the limit of vanishing phason self-action, the elasticity of quasicrystals is essentially standard elasticity in a space with dimension higher than the ambient one. However, there is a more subtle reason: if we look at the general analysis of configurational actions on cracks in complex media, as quasicrystals are, we realize that the energy release rate at a crack tip into a complex materials *does not include directly the self-action* (proofs are in [40,41]). The self-action has

only an indirect influence because it appears in the balance of micro-actions (here they are the phason ones), so the solutions take it into account.

By using equations (3.28) and (3.29), thanks to equations (3.22) and (3.23), we write

$$\mathcal{G} = \frac{1}{4}\sum_{k=1}^{2} \frac{K_k \bar{K}_k}{\cosh^2 \pi \gamma_k} \bar{\mathsf{w}}_k \cdot (Z + \bar{Z})\mathsf{w}_k,$$

after using the identity

$$\frac{1}{\hat{\lambda}} \int_0^{\hat{\lambda}} \sqrt{\frac{\varsigma}{\hat{\lambda} - \varsigma}} (\hat{\lambda} - \varsigma)^{i\gamma_k} \varsigma^{-i\gamma_k} \, \mathrm{d}\varsigma = \frac{\pi}{2} \frac{1 - 2i\gamma_k}{\cosh \pi \gamma_k},$$

and its conjugate [31,37]. Also, if we introduce a convenient normalization that prescribes

$$\bar{\mathsf{w}}_k \cdot \mathrm{D}\mathsf{w}_k = 1,$$

as suggested in [42], the energy release rate reduces to

$$\mathcal{G} = \frac{1}{2}\sum_{k=1}^{2} \frac{K_k \bar{K}_k}{\cosh^2 \pi \gamma_k}.$$

The two complex stress intensity factors depend on the normalization condition.

(d) Non-oscillatory fields

Consider the case in which Z is a real matrix. Equation (3.17) reduces to

$$\mathsf{h}^+(x) + \mathsf{h}^-(x) = 0, \quad \text{for } x < 0,$$

which admits the following normalized solution:

$$\mathsf{h}(z) = \frac{1}{2\sqrt{2\pi z}}\mathsf{k},$$

where k is the vector

$$\mathsf{k} = (K_{II}, K_I, T_{II}, T_I).$$

Thus, along the crack we have

$$\mathsf{t}_\mathrm{I} = \frac{1}{\sqrt{2\pi z}}\mathsf{k}, \quad \text{for } x > 0$$

and

$$i\mathsf{d}'(-x) = \frac{-i}{\sqrt{-2\pi z}} Z\mathsf{k}, \quad \text{for } x < 0.$$

By integration, we obtain

$$\mathsf{d}(-x) = 2\sqrt{\frac{-x}{2\pi}} Z\mathsf{k}, \quad \text{for } x < 0.$$

Then, the energy release rate reduces to

$$\mathcal{G} = \frac{1}{4}\mathsf{k} \cdot Z\mathsf{k}.$$

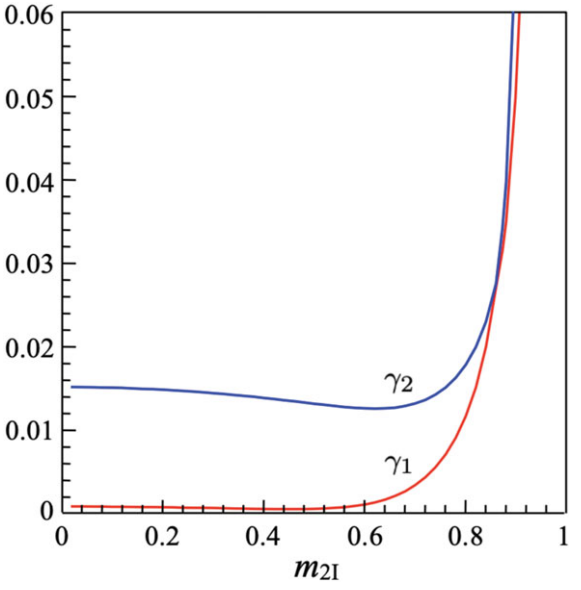

Figure 3. Variations of the oscillation indices γ_1 and γ_2, with the ratio m_{2I} between the crack-tip speed and the shear wave speed for material I.

(e) A special concrete case

We adopt the following values for the constitutive coefficients [43,44]:

$$\lambda_I = 85\,\text{GPa}, \quad \mu_I = 65\,\text{GPa}, \quad k_{1I} = 84\,\text{MPa}, \quad k_{2I} = 36\,\text{MPa}, \quad k_{3I} = 408\,\text{MPa},$$
$$\lambda_{II} = 74.9\,\text{GPa}, \quad \mu_{II} = 72.4\,\text{GPa}, \quad k_{1II} = 125\,\text{GPa}, \quad k_{2II} = -50\,\text{GPa},$$
$$k_{3II} = 951\,\text{GPa}.$$

The values of the coupling parameter k_3 correspond to $\chi_I = k_{3I}/k_{1I} = 4.85$ and $\chi_{II} = k_{3II}/k_{1II} = 7.61$. The experimental determination of the coupling parameter k_3 is uncertain, owing to the different order of magnitude between the amplitudes of phason and phonon fields.

The Rayleigh wave speeds for the two materials are given by the condition $\det \mathsf{H}_n = 0$ (for $n = \text{I}, \text{II}$) and correspond to $m_{2I} = 0.920$ and $m_{2I} = 0.917$, respectively.

The variations of oscillation indices γ_1 and γ_2 with the crack speed are shown in figure 3. The level sets of phonon and phason stress components are shown in figure 4. They refer to the crack-tip speed $m_{2I} = v/c_{SI} = 0.6$ and to any loading that determine the energy release rate defined at page 14 and stress intensity factors $K_1 = i$ and $K_2 = 0.1i$. The distributions of the standard stress fields are similar to those obtained for an interface crack propagating in classical elastic bi-material and display singular oscillatory behaviour very near to the crack tip. The phason stress field also displays a similar behaviour near the crack tip, even if its magnitude is much smaller than that of the standard stress. Figure 5 depicts the scenario in mode I conditions.

Eventually, figure 6 shows the way in which the determinant of $\mathbf{D}$ varies as the ratio m_{2I} increases. Figures 3–6—we repeat—refer to the closed-form solution in the case $\boldsymbol{\zeta} = 0$.

4. Analysis including the phason self-action

The same path is difficult to follow in the presence of a phason self-action. From a purely formal viewpoint, when $\boldsymbol{\zeta} \neq 0$ even in the simplest linear case, we shift from a problem of the type $\Delta w = 0$ to $\Delta w = \alpha w$, with some vector field w and scalar α; so, it is hard to directly apply Stroh formalism. In any case, beyond questions of convenience in the development of formal analyses, since the

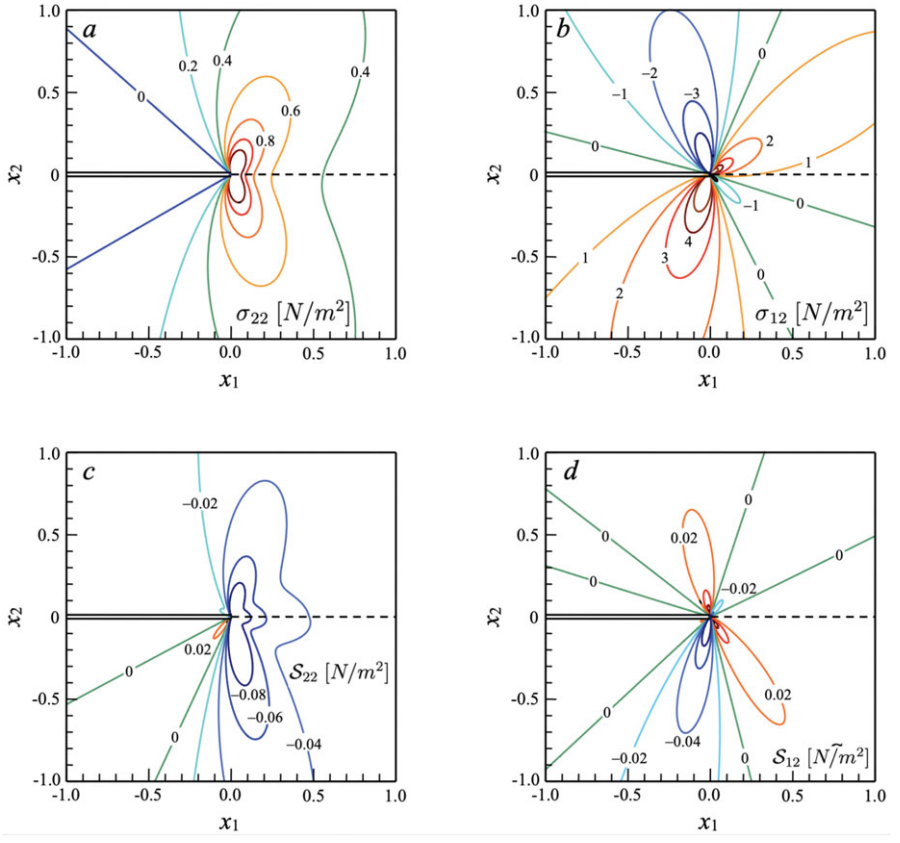

Figure 4. Variation of the phason and phonon stresses near the interface crack tip for a tip speed equal to $m_{2|} = v/c_{S|} = 0.6$ and the complex stress intensity factors $K_1 = i$ and $K_2 = 0.1i$.

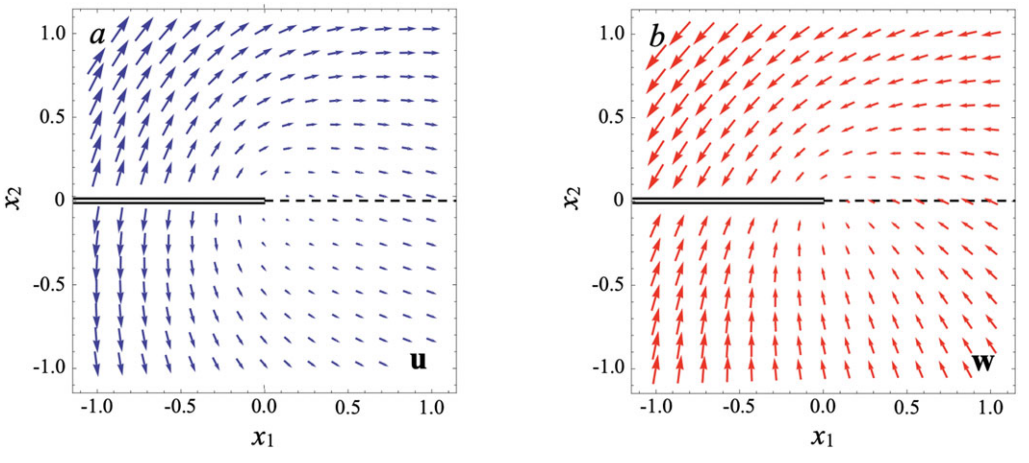

Figure 5. Distribution of the phason and phonon displacements near the tip for a speed equal to $m_{2|} = v/c_{S|} = 0.6$ and the complex stress intensity factors $K_1 = i$ and $K_2 = 0.1i$.

derivation of the balance equations for quasicrystals does not exclude the presence of a phason self-action, we need to account for it and to compare results with the case discussed above. Itself, the comparison with direct experiments based on the evaluation of the stress distribution on a bi-material plate which can indicate whether the particular constitutive choice to consider phasonic self-action null has a universal character or not.

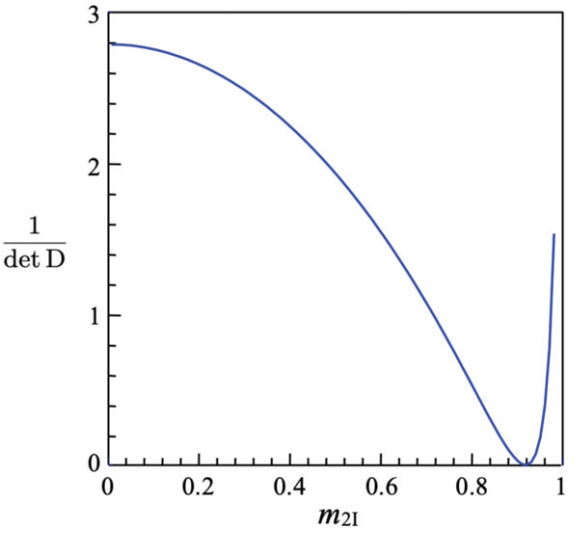

Figure 6. Variation of 1/det D versus the ratio m_{2I} between crack tip and shear wave speeds for material I.

We perform the analysis using standard finite elements and refer to statics; indeed, our aim is just to check the influence of $\boldsymbol{\zeta}$ on $\boldsymbol{\sigma}$ and $\mathcal{S}$ around the crack tip.

(a) Boundary conditions

We partition the boundary $\partial\mathcal{B}$ into two pairs of disjoint sets. Specifically, we choose $\partial\mathcal{B} = \partial\mathcal{B}^u \cup \partial\mathcal{B}^t$, with $\partial\mathcal{B}^u \cap \partial\mathcal{B}^t = \emptyset$ and $\partial\mathcal{B} = \partial\mathcal{B}^\nu \cup \partial\mathcal{B}^\tau$, with $\partial\mathcal{B}^\nu \cap \partial\mathcal{B}^\tau = \emptyset$; $\partial\mathcal{B}^u$ and $\partial\mathcal{B}^\nu$ are the parts of the boundary where essential boundary conditions are prescribed, and $\partial\mathcal{B}^t$ and $\partial\mathcal{B}^\tau$ are those where natural boundary conditions are assigned. Formally, possible boundary conditions are as follows:

$$u = \hat{u}, \quad x \in \partial\mathcal{B}^u,$$
$$\nu = \hat{\nu}, \quad x \in \partial\mathcal{B}^\nu,$$
$$\sigma n = \hat{t}, \quad x \in \partial\mathcal{B}^t$$

and

$$Sn = \hat{\tau}, \quad x \in \partial\mathcal{B}^\tau,$$

where $\hat{u}$ and $\hat{\nu}$ are prescribed vectors of phonon and phason degrees of freedom, respectively, $\hat{t}$ and $\hat{\tau}$ are prescribed phonon and phason tractions, respectively, and n is the unit vector normal to $\partial\mathcal{B}$. Indeed, the only reasonable choices for $\hat{\nu}$ and $\hat{\tau}$ at the external boundary are null, that is,

$$\hat{\nu} = 0 \quad \text{on } \partial\mathcal{B}^\nu \quad \text{and} \quad \hat{\tau} = 0 \quad \text{on } \partial\mathcal{B}^\tau,$$

because ν refers to degrees of freedom that are inside the material elements at continuum scale and we neither know nor imagine any loading device able to act directly on ν through the body boundary.

(b) Finite-element discretization

We start from the weak form of the balance equations involving test fields δu and $\delta\nu$ which belong to $H^1(\mathcal{B})$, that is, they admit weak derivatives that are square integrable, and vanish at the body

boundary. With $\mathfrak{t} = \boldsymbol{\sigma} n$ and $\tau = \mathcal{S} n$, where n is the outward unit normal to any oriented surface in $\mathcal{B}$, for any finite element $\mathfrak{b}$ in $\mathcal{B}$, we have

$$\int_{\mathfrak{b}} \nabla \delta u \cdot \boldsymbol{\sigma} \, \mathrm{d}x + \int_{\mathfrak{b}} \nabla \delta \nu \cdot \mathcal{S} \, \mathrm{d}x + \int_{\mathfrak{b}} \delta \nu \cdot \boldsymbol{\zeta} \, \mathrm{d}x = \int_{\partial \mathfrak{b}} \delta u \cdot \mathfrak{t} \, \mathrm{d}\ell + \int_{\partial \mathfrak{b}} \delta \nu \cdot \tau \, \mathrm{d}\ell, \tag{4.1}$$

where $\mathrm{d}\ell$ is the line measure.

The matrix notation used for the computations is given below. Displacement and phason degrees of freedom, their spatial derivatives, the relevant stresses and body forces are collected in the following vectors:

$$\mathbf{u} = \begin{bmatrix} u_1 \\ u_2 \end{bmatrix}, \quad \boldsymbol{\nu} = \begin{bmatrix} \nu_1 \\ \nu_2 \end{bmatrix}$$

$$D\mathbf{u} = \begin{bmatrix} \partial_1 u_1 \\ \partial_2 u_1 \\ \partial_1 u^2 \\ \partial_2 u_2 \end{bmatrix}, \quad D\boldsymbol{\nu} = \begin{bmatrix} \partial_1 \nu_1 \\ \partial_2 \nu_1 \\ \partial_1 \nu_2 \\ \partial_2 \nu_2 \end{bmatrix}$$

and

$$\hat{\boldsymbol{\sigma}} = \begin{bmatrix} \sigma_{11} \\ \sigma_{12} \\ \sigma_{21} \\ \sigma_{22} \end{bmatrix}, \quad \hat{\mathcal{S}} = \begin{bmatrix} \mathcal{S}_{11} \\ \mathcal{S}_{12} \\ \mathcal{S}_{21} \\ \mathcal{S}_{22} \end{bmatrix}, \quad \mathbf{t} = \begin{bmatrix} \mathfrak{t}_1 \\ \mathfrak{t}_2 \end{bmatrix}, \quad \boldsymbol{\tau} = \begin{bmatrix} \tau_1 \\ \tau_2 \end{bmatrix}, \quad \mathbf{b} = \begin{bmatrix} b_1 \\ b_2 \end{bmatrix}.$$

Also, we have

$$\begin{bmatrix} \hat{\boldsymbol{\sigma}} \\ \hat{\mathcal{S}} \end{bmatrix} = \begin{bmatrix} \boldsymbol{C} & \boldsymbol{K}' \\ \boldsymbol{K}'^{\mathrm{T}} & \boldsymbol{K} \end{bmatrix} \begin{bmatrix} D\mathbf{u} \\ D\boldsymbol{\nu} \end{bmatrix},$$

where

$$\boldsymbol{C} = \begin{bmatrix} \lambda + 2\mu & 0 & 0 & \lambda \\ 0 & \mu & \mu & 0 \\ 0 & \mu & \mu & 0 \\ \lambda & 0 & 0 & \lambda + 2\mu \end{bmatrix}$$

and

$$\boldsymbol{K}' = \begin{bmatrix} k_3 & 0 & 0 & k_3 \\ 0 & -k_3 & k_3 & 0 \\ 0 & -k_3 & k_3 & 0 \\ -k_3 & 0 & 0 & -k_3 \end{bmatrix}, \quad \boldsymbol{K} = \begin{bmatrix} k_1 & 0 & 0 & k_2 \\ 0 & k_1 & -k_2 & 0 \\ 0 & -k_2 & k_1 & 0 \\ k_2 & 0 & 0 & k_1 \end{bmatrix}.$$

Some points (finite in number) of $\mathcal{B}$ represent the integration nodes, where both displacement and phason degrees of freedom are controlled. The nodal values of the basic fields are collected in the vectors $\mathbf{U}$ and $\mathbf{V}$, respectively, and the interpolations

$$\mathbf{u}(x) = \mathbf{N}_u(x)\mathbf{U} \quad \text{and} \quad \boldsymbol{\nu}(x) = \mathbf{N}_\nu(x)\mathbf{V}$$

hold, where $\mathbf{N}_u$ and $\mathbf{N}_\nu$ are the matrixes of shape functions for the displacement and the phason degrees of freedom. We choose also the test fields in equation (4.1) to be such that

$$\delta\mathbf{u}(x) = \mathbf{N}_u(x)\delta\mathbf{U} \quad \text{and} \quad \delta\boldsymbol{\nu}(x) = \mathbf{N}_\nu(x)\delta\mathbf{V}.$$

With these notations, the virtual power identity equation (4.1), referred to a finite element $\mathfrak{b}$, reads

$$\begin{bmatrix} \mathbf{K}_{uu} & \mathbf{K}_{u\nu} \\ \mathbf{K}_{u\nu}^{\mathrm{T}} & \mathbf{K}_{\nu\nu} + \mathbf{A} \end{bmatrix} \begin{bmatrix} \mathbf{U} \\ \mathbf{V} \end{bmatrix} = \begin{bmatrix} \mathbf{F}_u \\ \mathbf{F}_\nu \end{bmatrix},$$

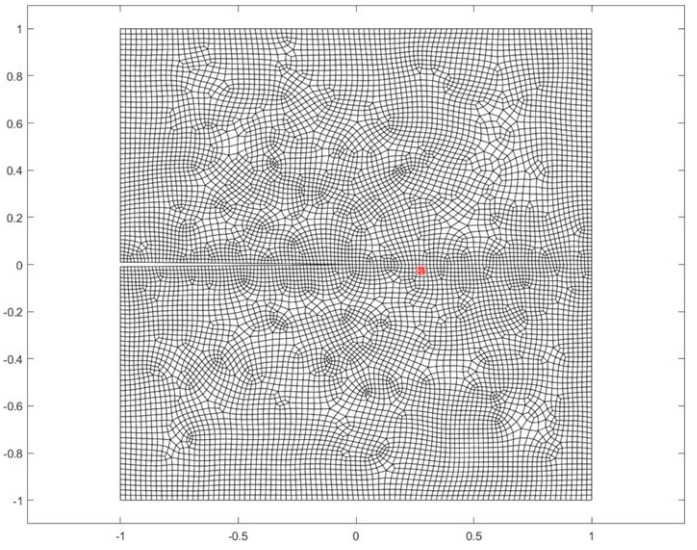

Figure 7. Mesh with quadrilateral elements (specimen size: 2m × 2m); the red element is the 5020th, where the internal power and the tangent matrix computed with Voigt's and intrinsic approaches have been compared, finding that they coincide.

where

$$\mathbf{K}_{uu} = \int_{\mathfrak{b}} (D\mathbf{N}_u)^{\mathrm{T}} \boldsymbol{C} (D\mathbf{N}_u)\, \mathrm{d}x, \quad \mathbf{K}_{u\nu} = \int_{\mathfrak{b}} (D\mathbf{N}_u)^{\mathrm{T}} \boldsymbol{K}' (D\mathbf{N}_\nu)\, \mathrm{d}x,$$

$$\mathbf{K}_{\nu\nu} = \int_{\mathfrak{b}} (D\mathbf{N}_\nu)^{\mathrm{T}} \boldsymbol{K} (D\mathbf{N}_\nu)\, \mathrm{d}x, \quad \mathbf{A} = \int_{\mathfrak{b}} \mathbf{N}_\nu^{\mathrm{T}} a I_4 \mathbf{N}_\nu\, \mathrm{d}x$$

and

$$\mathbf{F}_u = \int_{\partial\mathfrak{b}} \mathbf{N}_u^{\mathrm{T}} \mathbf{t}\, \mathrm{d}\ell, \quad \mathbf{F}_\nu = \int_{\partial\mathfrak{b}} \mathbf{N}_\nu^{\mathrm{T}} \boldsymbol{\tau}\, \mathrm{d}\ell.$$

At the external boundary, it is natural to assume $\mathbf{F}_\nu = 0$ while, inside the body, the phason traction is continuous at the finite-element interface.

We use standard quadrilateral elements with linear shape functions for both displacement and phason fields. The mesh, selected on a 2m × 2m specimen, is shown in figure 7. We refer to a standard finite-element approach because our focus is not on numerical methods, but rather on the will to explore differences in behaviour described by a scheme in which we foresee a phason self-action, although only with a conservative character, with respect to an analogous scheme in which the phason self-action is left out with a convenient reduction to standard elasticity, although in a higher-dimensional ambient setting. The above formulation in terms of Voigt's notation has been complemented by a parallel intrinsic approach for comparison. We report here only the numerical results obtained in terms of Voigt's notation. Convergence is achieved in a single iteration: in terms of norms, we move from 10^{-1} to 10^{-13} in one step. A uniformly distributed traction of $1\,\mathrm{N\,m^{-1}}$ is imposed at the top and bottom of the specimen in figure 7; they determine mode I conditions.

Figure 8 shows the maps of the standard vector norms $||u||$ and $||\nu||$; material parameters are those in §3e; the parameter determining the self-action $\boldsymbol{\zeta}$, that is, a, is taken to be equal to $1\,\mathrm{N\,m^{-4}}$. Figure 9 shows the isostress lines for the stress components σ_{22}, σ_{12}, $\mathcal{S}_{22}$ and $\mathcal{S}_{12}$. Differences with figure 4 are evident: $\boldsymbol{\zeta}$ increases the natural lack of symmetry around the crack, induced by the different nature of the materials on the two sides of the crack itself. For higher values of the self-action, the phason degrees of freedom are more and more frozen. We show in figures 10 and 11 the counterparts of figures 8 and 9 for $a = 2 \cdot 10^{12}\,\mathrm{N\,m^{-4}}$.

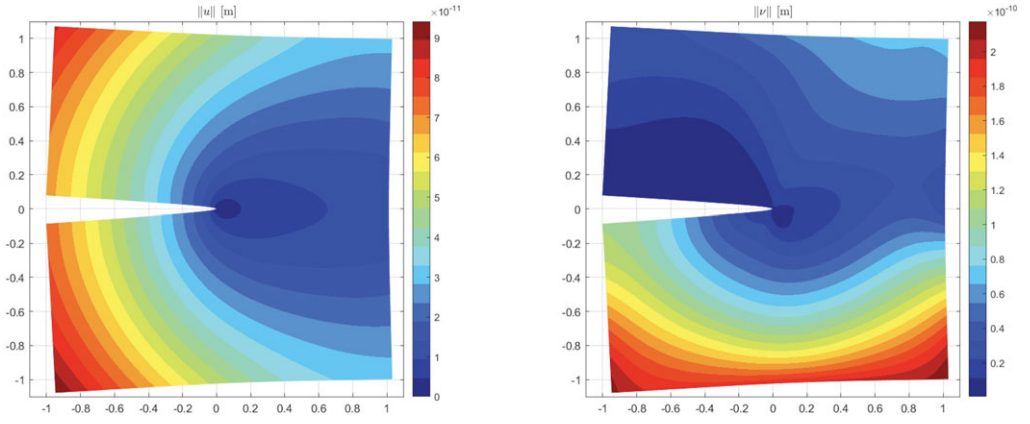

Figure 8. Distribution of displacement and phason field norms for a self-action coefficient $a = 1\,\mathrm{N\,m^{-4}}$ (specimen size: 2m × 2m).

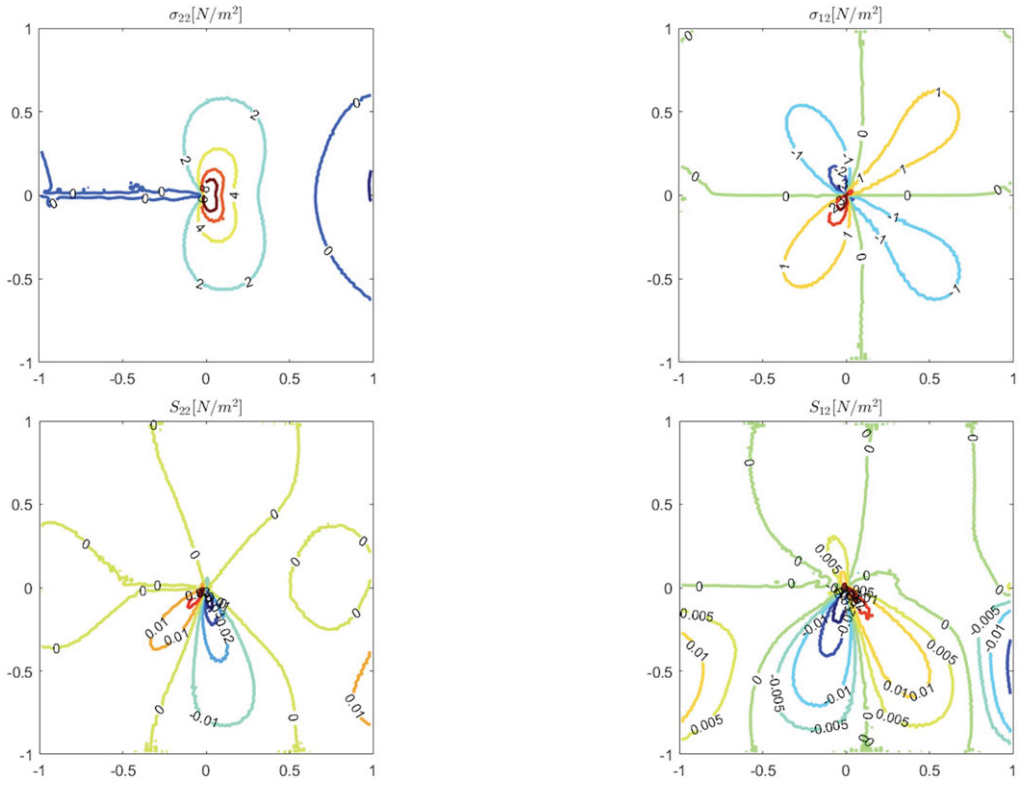

Figure 9. Standard and phason stress levels (isolines) under mode I loading conditions when $a = 1\,\mathrm{N\,m^{-4}}$ (specimen size: 2m × 2m).

5. Configurational forces at the crack tip

A general theory concerning the analysis of configurational forces on cracks in general complex bodies under large strains was presented in [40,41]. The structures of the emerging laws are irrespective of the specific nature of the microstructure, provided that they are represented by

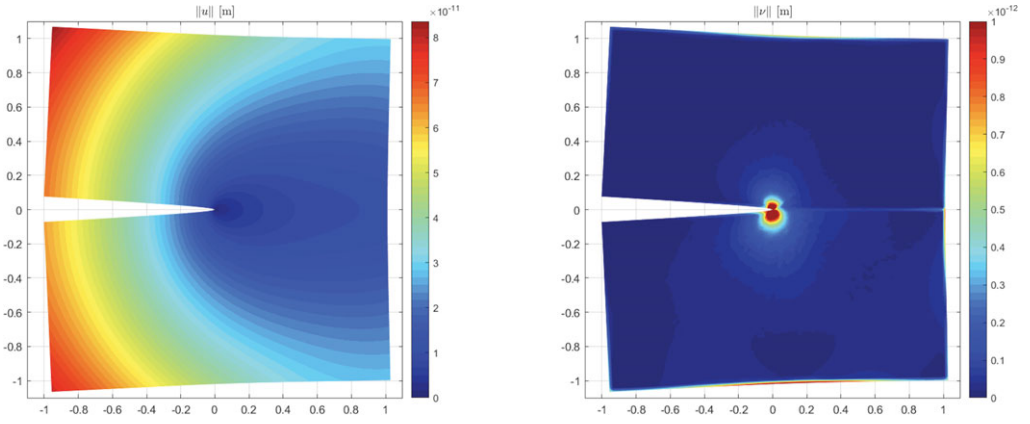

Figure 10. Distribution of displacement and phason field norms for a self-action coefficient $a = 2 \cdot 10^{12}$ N m^{-4} (specimen size: 2m $\times$ 2m).

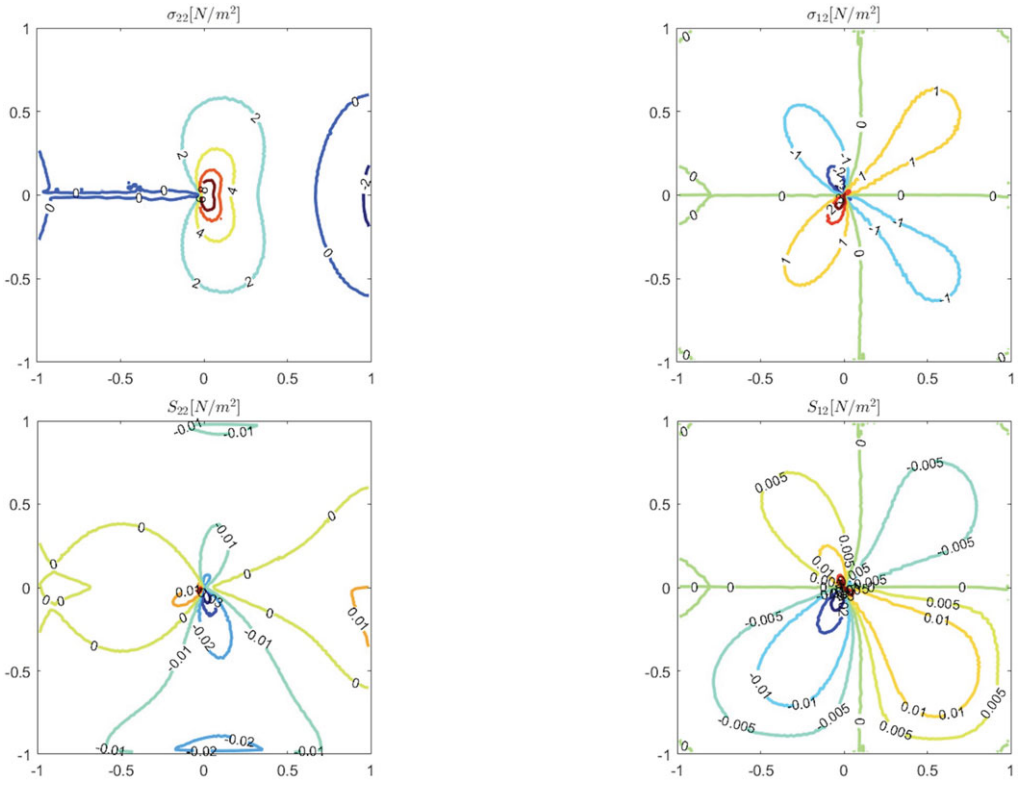

Figure 11. Standard and phason stress levels (isolines) under mode I loading conditions when $a = 2 \cdot 10^{12}$ N m^{-4} (specimen size: 2m $\times$ 2m).

phase fields (intended as descriptors of the material morphology on low spatial scales) that take values on spaces endowed at least with the geometric structure of a geodesic complete Riemannian manifold. Of course, $\mathbb{R}^3$ considered here has this geometric structure. Thus, we take from [41] essential conceptual elements derived there, reducing them to the small strain regime considered here.

For simplicity, we do not account for peculiar tip free energy; we merely consider the value ϕ of the surface energy density at the tip.

Consider a disc $\mathcal{D}_{\hat{\gamma}}$ with radius r, centred at the tip, with contour $\hat{\gamma}$. We indicate by n the outward unit normal to $\hat{\gamma}$ in the plane and by $\bar{n}$ its value parallel to the bi-material interface which, we recall, is planar. In the small strain setting considered here, the balance of configurational actions at the tip is given by

$$J - \phi = \mathfrak{g}_{\rm tip} \cdot \bar{n},$$

where $\mathfrak{g}_{\rm tip}$ is a configurational force on the tip while J is the version of J-integral that is appropriate for the present setting. It is given by

$$J := \bar{n} \cdot \lim_{r \to 0} \int_{\hat{\gamma}} (\mathbb{P} + \frac{1}{2}\rho|\dot{u} - (I + \nabla u)\mathfrak{v}_{\rm tip}|^2)n \, {\rm d}a,$$

where $\mathfrak{v}_{\rm tip}$ is the tip velocity with structure $\mathfrak{v}_{\rm tip} = V_{\rm tip}\bar{n}$, with $V_{\rm tip}$ a positive scalar and

$$\mathbb{P} = \psi {\rm I} - (\nabla u)^\top \boldsymbol{\sigma} - (\nabla v)^\top \mathcal{S}$$

is the Hamilton–Eshelby stress; da is the area measure (the superscript $\top$ indicates transposition). The tensor $\mathbb{P}$ satisfies in the bulk the local balance

$$\mathbf{div}\mathbb{P} - (I + \nabla u)^\top (b - \rho\ddot{u}) - \partial_x e + {\rm f} = 0,$$

where ∂_x indicates explicit derivative with respect to x, computed maintaining fixed all the state variables. The vector f is a bulk configurational force that is undetermined in the circumstance discussed here; we can set it equal to zero in the absence of material bond breaking outside the interface considered. Let m be the unit normal to the planar interface considered. Concerning the frame of reference in figure 2, m coincides with the unit vector of the x_2-axis. We indicate by $\mathbb{P}^+$ and $\mathbb{P}^-$ the limit values at the interface computed from the positive and negative orientation of m, respectively. As usual we denote by $[\mathbb{P}]$ the jump $\mathbb{P}^+ - \mathbb{P}^-$. Since the interface is planar, along it we have

$$m \cdot [\mathbb{P}]m = 0 \quad \text{and} \quad \bar{n} \cdot [\mathbb{P}]m = 0,$$

(see proofs in [41]).

Assume that the interface is weaker that the surrounding medium. Write ω for its strength, which we may assume to be constant imagining that the two half-planes are uniformly glued. According to a terminology adopted in [45], we say that $\mathfrak{g}_{\rm tip}$ is subcritical, critical or supercritical when, respectively,

$$\mathfrak{g}_{\rm tip} \cdot \bar{n} < \omega, \quad \mathfrak{g}_{\rm tip} \cdot \bar{n} = \omega, \quad \mathfrak{g}_{\rm tip} \cdot \bar{n} > \omega.$$

In this last case, we have evolution and the tip configurational balance becomes

$$J - \phi = \hat{\mathfrak{g}} V_{\rm tip},$$

with $\hat{\mathfrak{g}}$ is a positive constant.

In the setting sketched above, when inertia is absent and no bulk standard forces occur, since the interface is planar, the J-integral is path independent.

6. Concluding remarks

We have discussed the behaviour of cracks along planar interfaces between quasi-crystalline alloys in the small strain regime and with linear elasticity. When we neglect the phason self-action, we are able to furnish a closed-form solution under conditions of subsonic crack propagation. However, by finite-element analyses, we realize that the phason self-action can significantly alter the distributions of standard and phason stresses around the tip, although the self-action itself does not directly appear in the J-integral. Considering or avoiding the phason self-action in the elasticity of quasicrystals affects first and foremost qualitatively the stress distribution.

The techniques used in the present analysis can be adopted in other multi-field descriptions of bodies with different 'active' microstructures.

Data accessibility. This article does not contain any additional data.

Declaration of AI use. We have not used AI-assisted technologies in creating this article.

Authors' contributions. P.M.M.: conceptualization, formal analysis, investigation, methodology, supervision, writing—original draft, writing—review and editing; J.P.: conceptualization, formal analysis, investigation, supervision, validation, writing—review and editing; E.R.: conceptualization, formal analysis, investigation, methodology, validation, writing—original draft, writing—review and editing; L.S.: methodology, software, validation, visualization, writing—review and editing; M.M.S.: methodology, software, validation, visualization, writing—review and editing.

All authors gave final approval for publication and agreed to be held accountable for the work performed therein. Neither AI tools nor the help of third parties were used to write this article.

Conflict of interest declaration. We declare we have no competing interests.

Funding. This work belongs to activities of the research group 'Theoretical Mechanics' in the 'Centro di Ricerca Matematica Ennio De Giorgi', part of the Scuola Normale Superiore Pisa. GNFM-INDAM is acknowledged. M.M.S. acknowledges also the support from the Spanish Ministry of Science, Innovation and Universities (project no. PID2023-149658NB-I00).

References

1. Di Maida P, Radi E, Sciancalepore C, Bondioli F. 2015 Pullout behavior of polypropylene macro-synthetic fibers treated with nano-silica. *Constr. Build. Mater.* **82**, 39–44. (doi:10.1016/j.conbuildmat.2015.02.047)
2. Guinea GV, El-Sayed K, Elices M, Planas J. 2002 The effect of the bond between the matrix and the aggregates on the cracking mechanism and fracture parameters of concrete. *Cement Concrete Res.* **32**, 1961–1970. (doi:10.1016/S0008-8846(02)00902-X)
3. Radi E, Porcu MC. 2001 Near-tip fields for quasi-static crack growth along the interface between a porous-ductile material and a rigid substrate. *Int. J. Solids Struct.* **38**, 8235–8258. (doi:10.1016/S0020-7683(01)00142-1)
4. Shechtman D, Blech I, Gratias D, Cahn JW. 1984 Metallic phase with long-range orientational order and no translational symmetry. *Phys. Rev. Lett.* **53**, 1951–1954. (doi:10.1103/PhysRevLett.53.1951)
5. de Boissieu M, Boudard M, Hennion B, Bellissent R, Kycia S, Goldman A, Janot C, Audier M. 1995 Diffuse scattering and phason elasticity in the AlPdMn icosahedral phase. *Phys. Rev. Lett.* **75**, 89–92. (doi:10.1103/PhysRevLett.75.89)
6. Hu C, Wang R, Ding D-H. 2000 Symmetry groups, physical property tensors, elasticity and dislocations in quasicrystals. *Rep. Prog. Phys.* **63**, 1–39. (doi:10.1088/0034-4885/63/1/201)
7. Jeong H-C, Steinhardt PJ. 1993 Finite-temperature elasticity phase transition in decagonal quasicrystals. *Phys. Rev. B* **48**, 9394–9403. (doi:10.1103/PhysRevB.48.9394)
8. Thiel PA, Dubois JM. 1999 Quasicrystals. Reaching maturity for technological applications. *Mater. Today* **2**, 3–7. (doi:10.1016/S1369-7021(99)80058-3)
9. Rokhsar DS, Wright DC, Mermin ND. 1988 Scale equivalence of quasicrystallographic space groups. *Phys. Rev. B* **37**, 8145–8149. (doi:10.1103/PhysRevB.37.8145)
10. Mariano PM. 2002 Multifield theories in mechanics of solids. *Adv. Appl. Mech.* **38**, 1–93.
11. Mariano PM, Planas J. 2013 Self-actions in quasicrystals. *Physica D* **249**, 46–57. (doi:10.1016/j.physd.2013.01.006)
12. Mariano PM. 2006 Mechanics of quasi-periodic alloys. *J. Nonlinear Sci.* **16**, 45–77. (doi:10.1007/s00332-005-0654-5)
13. Mariano PM. 2024 Conducting viscous bodies with phase transitions: deriving Gurtin's postulate from the second law structure invariance. *Physica D* **467**, 134258. (doi:10.1016/j.physd.2024.134258)
14. Fan T. 2011 *Mathematical Theory of Elasticity of Quasicrystals and its Applications*, Science Press Beijing, Springer Verlag, Heidelberg.
15. Dang H, Lv S, Fan C, Lu C, Ren J, Zhao M. 2020 Analysis of anti-plane interface cracks in one-dimensional hexagonal quasicrystal coating. *Appl. Math. Model.* **81**, 641–652. (doi:10.1016/j.apm.2020.01.024)
16. Li H, Li W, Tan Y, Fan H, Wang Q, Li P. 2025 Phase-field modeling of interfacial fracture in quasicrystal composites. *Eng. Fracture Mech.* **314**, 110731. (doi:10.1016/j.engfracmech.2024.110731)

17. Li Y, Qin Q-H, Zhao MH. 2020 Analysis of 3D planar crack problems in one-dimensional hexagonal piezoelectric quasicrystals with thermal effect. Part I: theoretical formulations. *Int. J. Solids Struct.* **188–189**, 269–281. (doi:10.1016/j.ijsolstr.2019.10.019)
18. Li X-Y, Wang Y-W, Li P-D, Kang G-Z, Müller R. 2017 Three-dimensional fundamental thermo-elastic field in an infinite space of two-dimensional hexagonal quasi-crystal with a penny-shaped/half-infinite plane crack. *Theor. Appl. Fracture Mech.* **88**, 18–30. (doi:10.1016/j.tafmec.2016.11.005)
19. Zhao M, Fan C, Lu C, Dang H. 2021 Analysis of interface cracks in one-dimensional hexagonal quasi-crystal coating under in-plane loads. *Eng. Fracture Mech.* **243**, 107534. (doi:10.1016/j.engfracmech.2021.107534)
20. Benzi M, La Pegna D, Mariano PM. 2025 Spectra and pseudospectra in the evaluation of material stability in phase field schemes. *Eur. J. Mech. A/Solids* **112**, 105613. (doi:10.1016/j.euromechsol.2025.105613)
21. Govorukha V, Kamlah M. 2024 Analysis of an interface crack with multiple electric boundary conditions on its faces in a one-dimensional hexagonal quasicrystal bimaterial. *Arch. Appl. Mech.* **94**, 589–607. (doi:10.1007/s00419-024-02538-0)
22. Ma Y, Zhou Y, Yang J, Zhao X, Ding S. 2023 Interface crack behaviors disturbed by Love waves in a 1D hexagonal quasicrystal coating-substrate structure. *Z. Angew. Math. Phys.* **74**, 61. (doi:10.1007/s00033-023-01947-5)
23. Sladek J, Sladek V, Repka M, Schmauder S. 2023 Gradient theory of thermoelasticity for interface crack problems with a quasicrystal layer. *Int. J. Solids Struct.* **264**, 112097. (doi:10.1016/j.ijsolstr.2022.112097)
24. Wang X, Schiavone P. 2013 Dislocations, imperfect interfaces and interface cracks in anisotropic elasticity for quasicrystals. *Math. Mech. Comput. Syst.* **1**, 1–17. (doi:10.2140/memocs.2013.1.1)
25. Zhao M, Fan C, Lu CS, Dang H. 2022 Three-dimensional interfacial fracture analysis of a one-dimensional. *Appl. Math. Mech. Engl. Ed.* **43**, 1901–1920. (doi:10.1007/s10483-022-2927-6)
26. Zhang Z, Zhang B, Li X, Ding S. 2024 A closed-form solution to the mechanism of interface crack formation with one contact area in decagonal quasicrystal bi-materials. *Crystals* **14**, 316. (doi:10.3390/cryst14040316)
27. Stroh AN. 1962 Steady state problems in anisotropic elasticity. *J. Math. Phys.* **41**, 77–103. (doi:10.1002/sapm196241177)
28. Radi E, Mariano PM. 2011 Dynamic steady state crack propagation in quasi-crystals. *Math. Methods Appl. Sci.* **34**, 1–23. (doi:10.1002/mma.1325)
29. Morini L, Radi E, Movchan AB, Movchan NV. 2013 Stroh formalism in analysis of skew-symmetric and symmetric weight functions for interfacial cracks. *Math. Mech. Solids* **18**, 135–152. (doi:10.1177/1081286512462299)
30. Nobili A, Radi E. 2022 Hamiltonian/Stroh formalism for anisotropic media with microstructure. *Phil. Trans. R. Soc. A* **380**, 20210374. (doi:10.1098/rsta.2021.0374)
31. Suo Z, Kuo CM, Barnett DM, Willis JR. 1992 Fracture mechanics for piezoelectric ceramics. *J. Mech. Phys. Solids* **40**, 739–765. (doi:10.1016/0022-5096(92)90002-J)
32. Schmicker D, van Smaalen S. 1996 Dynamical behavior of aperiodic intergrowth crystals. *Int. J. Mod. Phys. B* **10**, 2049–2080. (doi:10.1142/S0217979296000933)
33. Bisconti L, Mariano PM. 2017 Existence results in the linear dynamics of quasicrystals with phason diffusion and nonlinear gyroscopic effects. *Multiscale Mod. Sim.* **15**, 745–767. (doi:10.1137/15M1049580)
34. Rochal SB, Lorman VL. 2002 Minimal model of the phonon-phason dynamics in icosahedral quasicrystals and its application to the problem of internal friction in the *i*-AlPbMn alloy. *Phys. Rev. B* **66**, 144204 (1–9). (doi:10.1103/PhysRevB.66.144204)
35. Maugin GA. 2016 A note on the thermo-mechanics of elastic quasi-crystals. *Arch. Appl. Mech.* **86**, 245–251. (doi:10.1007/s00419-015-1104-6)
36. Ding DH, Wang W, Hu C, Yang R. 1993 Generalized elasticity theory of quasicrystals. *Phys. Rev. B* **48**, 7003–7010. (doi:10.1103/PhysRevB.48.7003)
37. Suo Z. 1990 Singularities, interfaces and cracks in dissimilar anisotropic media. *Proc. R. Soc. Lond. A* **427**, 331–358. (doi:10.1098/rspa.1990.0016)
38. Yu HH, Suo Z. 2000 Intersonic crack growth on an interface. *Proc. R. Soc. Lond. A* **456**, 223–246. (doi:10.1098/rspa.2000.0515)
39. Irwin GR. 1957 Analysis of stresses and strains near the end of a crack traversing a plate. *J. Appl. Mech.* **24**, 361–364. (doi:10.1115/1.4011547)

40. Mariano PM. 2008 Cracks in complex bodies: covariance of tip balances. *J. Nonlinear Sci.* **18**, 99–141. (doi:10.1007/s00332-007-9008-4)
41. Mariano PM. 2025 Objectivity of the relative power and covariance of the Clausius-Duhem inequality in fracture dynamics. *Proc. R. Soc. A* **481**, 20240717. (doi:10.1098/rspa.2024.0717)
42. Hwu C. 1993 Explicit solutions for collinear interface crack problems. *Int. J. Solids Struct.* **30**, 301–312. (doi:10.1016/0020-7683(93)90167-6)
43. Edagawa K. 2007 Phonon–phason coupling in decagonal quasicrystals. *Phil. Mag.* **87**, 2789–2798. (doi:10.1080/14786430701264178)
44. Ricker M, Bachteler J, Trebin H-R. 2001 Elastic theory of icosahedral quasicrystals—application to straight dislocations. *Eur. Phys. J. B* **23**, 351–363. (doi:10.1007/s100510170055)
45. Gurtin ME, Podio-Guidugli P. 1996 Configurational forces and the basic laws of crack propagation. *J. Mech. Phys. Solids* **44**, 905–927. (doi:10.1016/0022-5096(96)00014-2)